Advanced Drug Delivery Reviews 65 (2013) 719–731

Contents lists available at SciVerse ScienceDirect

Advanced Drug Delivery Reviews

journal homepage: www.elsevier.com/locate/addr

Design of new quantum dot materials for deep tissue infrared imaging ☆

Elsa Cassette [a,1], Marion Helle [b,c,d,1], Lina Bezdetnaya [b,c,d], Frédéric Marchal [b,c,d,*], Benoit Dubertret [a,*], Thomas Pons [a,*]

[a] LPEM, ESPCI/CNRS/UPMC UMR 8213, 10, Rue Vauquelin, 75005 Paris, France
[b] Université de Lorraine, CRAN, UMR 7039, Campus Sciences, BP 70239, Vandœuvre-lès-Nancy Cedex, 54506, France
[c] CNRS, CRAN, UMR 7039, France
[d] Centre Alexis Vautrin, CRLCC, avenue de Bourgogne, Vandœuvre-lès-Nancy Cedex, 54511, France

ARTICLE INFO

Article history:
Accepted 24 August 2012
Available online 6 September 2012

Keywords:
Near infrared fluorescence
In vivo imaging
Quantum dots
Nanocrystals

ABSTRACT

Near infrared fluorescence offers several advantages for tissue and *in vivo* imaging thanks to deeper photon penetration. In this article, we review a promising class of near infrared emitting probes based on semiconductor quantum dots (QDs), which have the potential to considerably improve *in vivo* fluorescence imaging thanks to their high brightness and stability. We discuss in particular the different criteria to optimize the design of near infrared QDs. We present the recent developments in the synthesis of novel QD materials and their different *in vivo* imaging applications, including lymph node localization, vasculature imaging, tumor localization, as well as cell tracking and QD-based multimodal probes.

Contents

1. Introduction

The field of biomedical optics has matured rapidly during the last ten years, and is expected to continue its maturation even further in the next few years. The use of photons as a source of information to diagnose or to treat is as old as medicine. Together with the touch, photon detection, first performed with the eye, provides a rapid, immediate and cheap

☆ This review is part of the *Advanced Drug Delivery Reviews* theme issue on "Inorganic nanoparticle platforms".

* Corresponding authors.
E-mail addresses: f.marchal@nancy.fnclcc.fr (F. Marchal), benoit.dubertret@espci.fr (B. Dubertret), thomas.pons@espci.fr (T. Pons).

[1] These authors contributed equally to this work.

0169-409X/$ – see front matter © 2012 Elsevier B.V. All rights reserved.
http://dx.doi.org/10.1016/j.addr.2012.08.016

method for diagnosis and patient treatment. In spite of these great advantages, biomedical optics is strongly limited because photons are scattered and absorbed very efficiently by the tissues. The penetration depth of photons inside a tissue depends strongly on the type of tissue [1], but most importantly, it depends on the wavelength, λ, of the photon used. Scattering decreases proportionally to λ^{-a}, where a depends on the tissue composition. Absorption is minimal between 700 nm and 1300 nm. Before 700 nm various proteins such as hemoglobin absorb strongly, while after 1300 nm water absorption becomes dominant. This spectral range is usually separated into two distinct NIR windows [1,2]. The first and most commonly used near infrared (NIR) optical window of optimal transparency lies in the range of 700–950 nm. The other NIR window extends from 1000 nm to 1300 nm and is often referred to as the second optical window for *in vivo* imaging. However, there have been so far few biocompatible fluorophores emitting in this region. In these NIR regions, the photons can be detected at much greater tissue thicknesses, and observation can be performed at greater depth. Excitation and/or emission in the NIR window result in lower background fluorescence, lower signal loss and thus greater signal/background ratio. Unfortunately, the eye sensibility decreases abruptly after 700 nm, so that NIR photons are badly—if at all—detected by the human eye in the NIR window.

Recent technological developments have helped triggered a renewed interest in biomedical optics. These developments include cheap NIR photon sources such as laser diodes in the NIR, cheaper and efficient NIR detector, as well as novel NIR probes.

The review we present here is dedicated to the recent development of NIR emitting semiconductor nano-particles known as quantum dots (QDs), and their applications in biomedical imaging, with an emphasis on the design of optimal NIR emitting QDs. Because biomedical optics is rapid, portable and cheap, we expect that it will expand greatly in the next few years, especially if bright, stable, NIR emitting probes with low toxicity can be synthesized.

We can distinguish two classes of NIR emitting probes: organic and inorganic ones [3]. The NIR organic probes are the oldest and some of them (indocyanine green, methylene blue) have been validated by the US Food and Drug Administration (FDA) for use *in vivo*. NIR organic dyes suffer however from important limitations in terms of optical properties: their fluorescence quantum yield is low, they photobleach rapidly, and the possible emission wavelengths are limited to the high energy range of the NIR window (700–900 nm). Recently, certain of these limitations have been circumvented thanks to the encapsulation of the organic dyes in small beads such as lipoproteins nanoparticles [4], calcium phosphate nanoparticles [5–7], or dye doped silica nanoparticles [8–10].

Inorganic NIR emitting probes include QDs and up-converted nanoparticles. Metallic nanoparticles [11] and nanoshells [12] can be good NIR absorbing probes but, except from few recent examples [13], are usually not fluorescent in the NIR and will not be discussed here.

QDs are semiconductor particles with sizes that range from 2 nm to ~10 nm. As in the case of QDs emitting in the visible, the emission wavelength of the NIR QDs can easily be tuned between 650 nm and 1250 nm by changing their size or their composition. The notable optical properties of the NIR QDs are: i) good resistance to photobleaching (this is especially true when core/shell structures can be synthesized), ii) large absorption cross section, iii) Gaussian emission profiles with full widths at half maximum (FWHM) that can be as narrow as 40 nm [14], iv) fluorescence lifetime in general larger than 100 ns, v) good quantum yield that can be as large as 50%, and v) fluorescence emission with a large Stokes shift. These properties make the NIR QDs attractive compared to organic NIR probes [15].

In general, QDs are excited using one photon excitation, but they can also be excited using two photon (2P) absorption, a process with the simultaneous absorption of two photons exciting a transition at twice the energy of the incident photons. Their large two photon absorption cross section, compared to organic dyes, makes them very interesting probes for 2P excitation [16]. This type of excitation is interesting because it can be done in the NIR window and because it provides intrinsic three-dimensional confinement of the excitation inside a micrometer volume. It is thus well adapted to depths smaller than typically 400–500 μm [17].

Recently, another type of multi-photon absorbing probes has been evidenced with the lanthanide doped nanoparticles that can upconvert low energy NIR radiation into higher energy visible luminescence [18]. The luminescence of these up-converted nanoparticles is based on sequential energy transfers between lanthanide dopants or excited state absorption involving their metastable-excited states with lifetimes as long as several milliseconds. This process is orders of magnitude more efficient than the 2-photon absorption process typically used in 2P microscopy.

In depth fluorescence detection with greater signal/background ratio can also be performed using fluorescent probes that do not need to be excited with light when they are in the tissue. These probes can be excited by luciferase [19] through energy transfer, or when they have long fluorescence lifetime, they can be first excited *in vitro*, injected, and detected at later time [20].

2. QD synthesis

Several recent comprehensive reviews have already discussed the synthesis and the applications of NIR QDs [21–24], and the reader is encouraged to read these references for detailed discussion of the various synthesis protocols used. In the present review, we have chosen to focus on the design issues necessary to obtain the ideal NIR emitting QDs as well as the strategies currently available to fulfill them.

The main parameters that have to be taken into consideration when designing a NIR emitting QD are: i) the excitation and the emission wavelengths, ii) the toxicity of the elements the QD is made of, iii) the ability to transfer the probe into water, and to modify its surface chemistry without losing the QD fluorescence, iv) the brightness of the probe, i.e. its quantum yield, its absorption cross-section, its lifetime, its resistance to photobleaching, and v) the QD size.

Ideally, a NIR QD has an emission wavelength in the NIR window, where they may also be efficiently excited. It should be non toxic. However, the QD toxicity is a complex issue, as it strongly depends on its composition and on its surface chemistry, which determines its biodistribution. While QDs based on heavy metals may be used for short term imaging in the small animal, long term studies should use less toxic QD compositions to avoid possible side effects. This requirement naturally becomes a non sufficient, but absolutely necessary condition for eventual future clinical applications.

It should also be bright, although this notion is not easy to optimize and depends strongly on the type of excitation and detection that is performed. For continuous excitation, a shorter fluorescence lifetime is preferable since it ultimately limits the rate of fluorescence photons from the QD when excited at its saturation level. In contrast, a longer fluorescence lifetime is more advantageous in pulsed excitation/time-gated detection schemes, where the fluorescence is recorded during a specific time window after each excitation pulse. This allows the selective detection of late fluorescence photons emitted by long lifetime (hundreds of nanoseconds) QDs while rejecting early photons emitted by short lifetime (few ns) endogenous fluorophores. The QD size should be as small as possible since small sizes are optimal for renal clearance [25], although for some applications, larger sizes are desirable (see below).

Another important point yet needs to be considered in the design of a NIR emitting QD for bio-imaging. It is the robustness of its fluorescence emission in time, when excited (resistance to photobleaching), or when its surface chemistry is altered. Surface chemistry modifications can simply result from aging of the QDs under ambient conditions. Water and/or oxygen can bind to the QD surface and modify its fluorescence [26]. Further, to make the QD water soluble, surface chemical

modifications need to be performed. These modifications often degrade the fluorescence quantum yield of the QDs. The most efficient strategy found so far to preserve a good fluorescence is to grow a shell on the QD [27]. Such a shell needs to have a large bandgap to prevent the electron and the hole to reach the surface (type I). Ideally, this shell should be grown epitaxially to prevent cracks and charge leaks. While shell thickness is not critical, few monolayers are usually necessary to preserve a good fluorescence after ligand exchange.

It is however not easy to grow epitaxially a shell on a nanostructure. There are two major issues. The first one is the difference of the lattice constant parameters between the core and the shell. Lattice mismatch between the core and the shell results in pressure that can reach 4 GPa [28]. Such high pressure can induce crystal structure change, or defect formations in the core, the shell or both. When the lattice mismatch is too high, gradient composition between the core and the shell can be designed so that the constraints can be slightly relaxed and shells grown with fewer defects. The second major issue when growing a shell on a QD core is to prevent diffusion of the anion and/or the cation into the core during the shell growth that is usually performed at high temperature (>200 °C). Such diffusion can change drastically the emission wavelength of the QDs, and its surface can fail to be correctly passivated by the shell. ZnS represents the archetypical shell material, due to its good resistance to oxidation and to the position of its bandgap conveniently enclosing that of most NIR emitting QDs.

The emission wavelengths of a NIR QDs can be easily tuned by changing their composition (Table 1).

2.1. Group IV (Si, Ge, C)

Group IV nanocrystal quantum dots are composed of only one element, Si, Ge or C. These semiconductors play a major role in electronics, and the synthesis of the corresponding QDs has been attracting increasing interest and effort [42,43]. Their PL emission may originate from either band edge or defect states.

Various synthetic routes have been developed to obtain Si QDs, such as electrochemical etching, laser ablation, mechanical milling and plasma synthesis [42]. Recent synthesis schemes reported 800 nm-emitting Si QDs with quantum yields up to 60–70% in organic solvents however these QDs were unstable in water [44,45]. The surface of Si QDs is usually stabilized with appropriate covalently bound organic ligands, and the resulting NIR-emitting QDs reach a quantum yield of 5–20% after solubilization in water [30,46,47]. Alternatively, luminescent porous Si nanoparticles, with overall diameters of ~130 nm and inner pores ~5–10 nm, were prepared by electrochemical etching [48]. These particles emitted in the 700–900 nm window with 10% quantum yields. Interestingly, the authors demonstrated that these porous particles could be loaded with drugs, and that they progressively degraded and dissolved *in vivo* into soluble silicic acid, followed by fast excretion (see Fig. 1). However these QDs could only be excited in the visible region, which could limit the available imaging depth [46].

Germanium QDs have been synthesized in solution [49,50] or by dissolution of processed sol–gel glasses [51], with peak emission wavelengths ranging from ~800 to ~1200 nm and quantum yields varying from 0.05% to 8% depending on the size and the synthetic scheme. They therefore offer a broader NIR emission range but no core/shell structure has been reported on Ge QDs yet and they remain very sensitive to oxidation. These QDs have thus not been transferred into water for biological imaging purposes.

Finally, diamond nanoparticles have a very wide bandgap, however defect states may fluorescence in the visible or the NIR region. For example, Si and Ni–N defects provide PL emission lines in the 700–800 nm region [52,53]. However these nanodiamonds cannot be excited in the near infrared region and their surface functionalization for biological imaging raises challenges that delay their application for bioimaging.

NIR QDs containing two elements are so far the most widely synthesized. We will review rapidly their properties according to the cation they contain: Ag, Cd, Pb or In.

2.2. Group I–VI (Ag_2S, Ag_2Se, Ag_2Te)

Ag_2S, Ag_2Se, and Ag_2Te QDs have only recently been synthesized. The group of D. Norris has shown that these nanoparticles can be easily synthesized using classical methods, but their study does not report on the photoluminescence properties of these nanoparticles [54]. Another study used a silylamide promoted synthesis to obtain Ag_2E (E = S, Se, Te) QDs. These QDs have detectable fluorescence emission, but their quantum yield remains low (few %) even after the growth of ZnSe shells. The emission wavelength of these nanoparticles can be tuned across the NIR window [55], but the FWHM of their emission spectra is very large (>200 nm). The lifetimes reported so far are a bit longer than 100 ns. Finally, matchstick-shaped Ag_2S–ZnS heteronanostructures have recently been synthesized with both UV and NIR emission at 1155 nm, however no fluorescence quantum yield was measured [56].

2.3. Groups II–VI and II_3–V_2

CdSe and CdTe nanoparticles are limited to the high energy part of the NIR window (up to ~700 nm for CdSe [57] and ~800 nm for CdTe [58]). These nanoparticles can have an emission spectra with narrow FHWM (30 nm), short lifetime (few tens of ns), and quantum yield that strongly depend on their surface state. Even though their syntheses are well documented [59], cadmium based NIR nanoparticles are still the subject of active research.

The synthesis of core/shell structures with CdSe or CdTe cores requires some special care. An ideal shell material for these two types of core in terms of band alignment and resistance to photobleaching would be ZnS. However, the lattice mismatch between CdSe (14%) and CdTe (17%) prevents the formation of thick shells (more than 2 monolayers), and strategies usually based on the use of composition gradient, or intermediate materials, between the core and the shell, are used to build adapted core shell structures as in the case of CdSeTe/CdZnS [31].

Wave function engineering can be used to obtain core/shell NIR emitting QDs. The idea here is to use semiconductor materials for the core and the shell such that the electron and the hole are mostly localized in different parts of the nanoparticle. These QDs are called type II QDs. The first example of such NIR emitting QDs is the CdTe/CdSe QD, where the electron is mostly localized in the shell while the hole is mostly confined in the core [34]. This wave function engineering with the charges localized in different parts of the QD results in reduced confinement of the charge carriers, and thus

Table 1
Water soluble NIR emitting quantum dots of various materials with their emission range and their quantum yield. We limited this table to NIR emitting QDs that have been solubilized in water. Only one or two representative examples for each material are given.

	Emission range	Full width half maximum	Quantum yield in water
C [29]	650–700 nm	~100 nm	N.A.
Si [30]	650–700 nm	>100 nm	5%
CdSeTe/CdZnS [31]	650–800 nm	<100 nm	25–30%
CdTe/CdSe/ZnSe [32]	900–1000 nm	>100 nm	50%
CdTe/CdS [33]	650–800 nm	<100 nm	up to 70%
CdTe/CdSe [34]	840–860 nm	90 nm	13%
$CuInS_2$/ZnS [35,36]	650–820 nm	~100 nm	~30%
$CuInSe_2$/ZnS [37]	700–1050 nm	>100 nm	~20%
InAs/ZnCdS [38]	700–800 nm	80 nm	25%
InAs/ZnS [39]	750 nm	<100 nm	10–20%
InP/ZnS [40]	650–740 nm	150 nm	15%
PbS/CdS [41]	1250 nm	~150 nm	30%

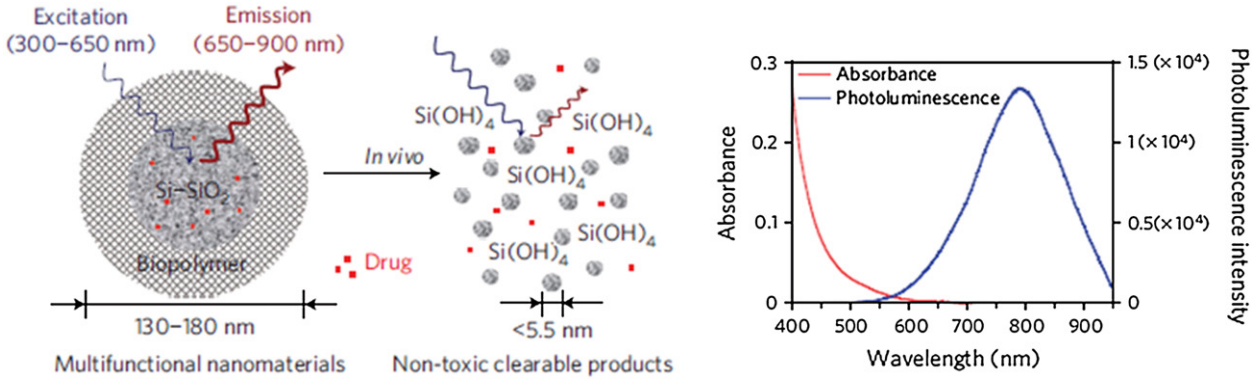

Fig. 1. Structure, degradation process and optical spectra of NIR emitting porous silicon nanoparticles. Reproduced with permission from Macmillan Publishers Ltd: Nature Materials [48] copyright (2009).

longer emission wavelengths. The reduction of the wave-function overlap also results in longer fluorescence lifetimes. Several core/shell structures with bandgap alignment resulting in longer emission wavelength have been synthesized since [60], and core/shell structures of type II/type I QDs that can be transferred into water have been synthesized [32]. A refinement of type II QDs is the use of lattice strain to fine tune the band alignment between the core and the shell. The epitaxial growth of a compressive shell onto a soft nano-crystalline core could induce a switch between a standard type-I QD and a type-II QD [14]. This method has the advantage to give NIR emitting QDs with high quantum yield, and emissions with a narrow (~40 nm) full width half maximum.

An extension of the type II QDs is the nanoparticle, composed of a gradient in the QD itself, usually at the interface between the core and the shell. Such composition gradient gives access to various core/shell structures that would be hard to grow otherwise because of the often large lattice mismatch between the core and the shell [31]. Composition gradient can also be obtained after synthesis using cation exchanges [61].

Recently, Cd_3P_2 [62,63] and Cd_3As_2 [64] QDs with emission in the full NIR window have been synthesized. These QDs can have quantum yields higher than 30% after the synthesis but, as most NIR QDs, this value drops dramatically after few days in ambient conditions [64]. The FWHM of these QDs increases with particle size from 80 nm to 150 nm. These materials would benefit from the addition of a shell so that they can be used for biomedical imaging.

2.4. Group IV–VI (PbS, PbSe)

PbS, PbSe and PbTe nanoparticles are probably the oldest NIR absorbing QDs synthesized [65]. These materials have very small bandgaps <0.5 eV, but large Bohr radii, 20 nm for PbS, 46 nm for PbSe [66]. As a consequence, their emission spectra can be easily tuned in the middle and the low energy part (infrared) of the NIR window. The quantum yield of these QDs varies greatly according to their synthesis. Recent synthesis optimization has led to air stable PbS nanoparticles with excellent quantum yields (up to 90%) [67]. The FWHM of these QDs depends on their size but is in general very large (>100 nm). Their fluorescence lifetime is long, and often close to the microsecond [68]. The fluorescence stability of PbS and PbSe nanoparticles can be greatly enhanced using core/shell structures such as PbSe/CdSe/ZnS and PbS/CdS [69]. The quantum yield of these structures remains high (~20–30%) even after transfer into water [41]. The FWHM of their emission is still large (>200 nm).

2.5. Group III–V (InP, InAs)

As for the QDs containing indium, they have first been synthesized more than 15 years ago both as InP [70,71] and as InAs QDs [72]. InP QDs have triggered a great deal of attention since the InP bandgap is 1.35 eV (~920 nm), so that large InP QDs can reach the high energy part of the NIR window, but more importantly, the compounds these QDs are made of are expected to be less toxic than other heavy metals. Core/shell InP/ZnS nanoparticles have been synthesized [73] and recent optimization yielded stable water soluble InP/ZnS NCs with quantum yield around 15% [40]. Longer wavelength can be reached with InAs QDs. The InAs bandgap is 0.53 eV (>3 μm), and the first InAs QDs synthesized [70] cover the whole NIR window. Different kinds of shell have been grown on InAs cores. The first shells were based on the selenides, specifically ZnSe and CdSe [74–76], but selenium is prone to oxidation, and air stable sulfides have subsequently been used. ZnS [39,77] has a high lattice mismatch (10.7%) with InAs and ZnS shells are thus difficult to grow. Recently, CdS and ZnCdS shells have been synthesized on InAs cores yielding QDs that are stable in air and can be transferred into water using ligand exchange. These QDs retain high quantum yield (25%) once in water [38]. They have been synthesized only for the high energy part of the NIR window (700–800 nm), but longer wavelength should easily be accessible with larger core sizes. The FWHM of these samples is quite narrow (<100 nm).

2.6. Group I–III–VI$_2$ ($CuInS_2$, $CuInSe_2$, $AgInSe_2$)

Ternary QDs have recently emerged as a new class of NIR emitters. As for the QDs containing Ag, the development of these materials was motivated by the need to synthesize NIR QDs with elements that are available in large quantities and with reduced toxicity [35]. Examples of ternary NIR QDs are $CuInS_2$, $CuInSe_2$, and $AgInSe_2$. We discuss below the properties of these QDs since they have only been recently applied to biological imaging and have therefore not been covered by previous reviews.

The recent renewed interest for the synthesis I–III–VI$_2$ nanoparticles comes from the fields of both photovoltaics and biomedical imaging. NCs with a wide range of sizes have been synthesized for both $CuInS_2$ and $CuInSe_2$ [35–37,78–83]. The Bohr radii of $CuInS_2$ and $CuInSe_2$ are respectively 3.9–4.1 nm and 5.43 nm, and the bandgap energies are respectively 1.45–1.53 eV and 1.04 eV. In $CuInS_2$ and $CuInSe_2$ structure, the ratio In/Cu is one, on average, and the negative charges of the S or Se (−II) anions compensate the positive charges of the cations In (+III) and Cu (+I). However, the Cu–In–S/Se materials are well known to present a large variety of Cu/In ratios [37,78,84,85], because of the stability of various pairs of defects [85]. For example, indium-rich nanocrystals are obtained when 2 copper vacancies are combined with the substitution of one indium on a copper site ($In_{Cu}^{2+} + 2V_{Cu}^{-}$) and copper-rich NCs are obtained when one indium is substituted with two coppers, and one copper is substituted with one indium ($2Cu_{In}^{2-} + In_{Cu}^{2+}$). Thus, stable In- or Cu-rich Cu–In–S/Se NCs can be synthesized. Nanoparticles that have higher In/Cu ratio have larger bandgap energy and all wavelengths from green–yellow to NIR (~810 nm for $CuInS_2$ and ~1190 nm for $CuInSe_2$) can be obtained using various NC

sizes and compositions (Fig. 2) [35–37,78,80,81,83,84,86]. It is interesting to note that bigger particles (>5 nm) are less fluorescent than smaller ones, because the number of internal defects scales with the volume of the particles. As a consequence, for a given emission wavelength, it can be preferable to use smaller Cu–In–Se particles than larger Cu–In–S [37].

When the In and Cu cations alternate periodically in the crystal lattice, $CuInS_2$ and $CuInSe_2$ NCs have a chalcopyrite crystal structure. In contrast, when the cations are randomly positioned in the crystal, the structure is sphalerite (zinc blende). The I–III–VI_2 NCs have usually tetrahedral or spherical shape, depending on the synthesis used, although other shapes have been synthesized but no fluorescence emission was reported for these NCs. Prasad et al. [87] have reported the synthesis of fluorescent Cu–In–S/ZnS NCs in the anisotropic wurtzite structure. This paves the way to the design of QDs with anisotropic shapes (rods, plates…) and special optical properties (e.g. polarized emission).

The absorption spectra of I–III–VI_2 NCs do not display excitonic structure (Fig. 2e) because the NC dispersion in size and composition is too important. The PL spectra are broad (full width at half maximum: 100–150 nm). This width was attributed to the large NC dispersion in size and composition along with the recombination of the exciton with defect levels inside the nanoparticles [37,79,84,88]. Exciton recombination at defect sites also results in emission at lower energy, which can result in emission at wavelengths higher than for the bulk material, see Fig. 2a, and longer fluorescence lifetime (few hundred nanoseconds).

To improve the robustness of the optical properties of the I–III–VI_2 NCs, core/shell structures have been synthesized with shells of zinc sulfide [35–37,84,87–89]. Zinc sulfide has a large bandgap (3.61 eV) that provides a type I-alignment with $CuInS_2$ and $CuInSe_2$ cores, does not contain heavy metals, is stable against oxidation and has a small lattice mismatch with the core material (2% with $CuInS_2$ and 7% with $CuInSe_2$), so that epitaxial growth of several monolayers is possible.

Although very favorable in principle, the growth of a ZnS shell on I–III–VI cores turns out to be difficult in large part because of the easy diffusion of the small Zn^{2+} cation into the core against its reactivity. ZnS shells can eventually be grown if more reactive precursors are used and if the shell is grown at lower temperatures (≤200 °C). However, at this time, only few monolayers of pure ZnS shell have been reported in the literature. After the growth of a ZnS shell, the NC fluorescence quantum yield (QY) increases to a maximum of 60% in the visible range and ~30% in the NIR [35–37,84,87–89]. This increase is accompanied by the disappearance of the fast lifetime component, related to exciton non radiative decay on a surface defect [36,86]. Long (few hundred ns) mono-exponential fluorescence lifetime can then be obtained (Fig. 2d).

Other NIR I–III–VI materials have recently emerged, such as $AgInSe_2$ but no fluorescent core/shell nanostructures have been reported yet.

I–III–VI_2 core/shell NCs have comparable or higher QY than NIR organic dyes one, but their photo-stability and their absorption cross section are much larger. Despite their complexity (ternary composition and presence of defects), these NCs represent promising materials for *in vivo* imaging, as recently reported [35–37,87,89].

2.7. NIR emitting doped nanocrystals

The previous section shows that the whole NIR window can be explored when the composition and/or the size of the nanoparticles is changed. Another method yet to tune the emission wavelength of QDs is to dope them. Doping has been studied in details for QDs emitting in the visible [90]. Doped NIR emitting QDs have recently been synthesized [91], and their emission wavelength can be tuned continuously almost in the entire NIR window. These QDs could offer an interesting alternative to existing NIR QDs in terms of toxicity.

When we combine the possibility to change the QD composition with the ability to grow core/shell structures, a large variety of water soluble, NIR emitting QDs can be synthesized, with emission wavelengths tuning

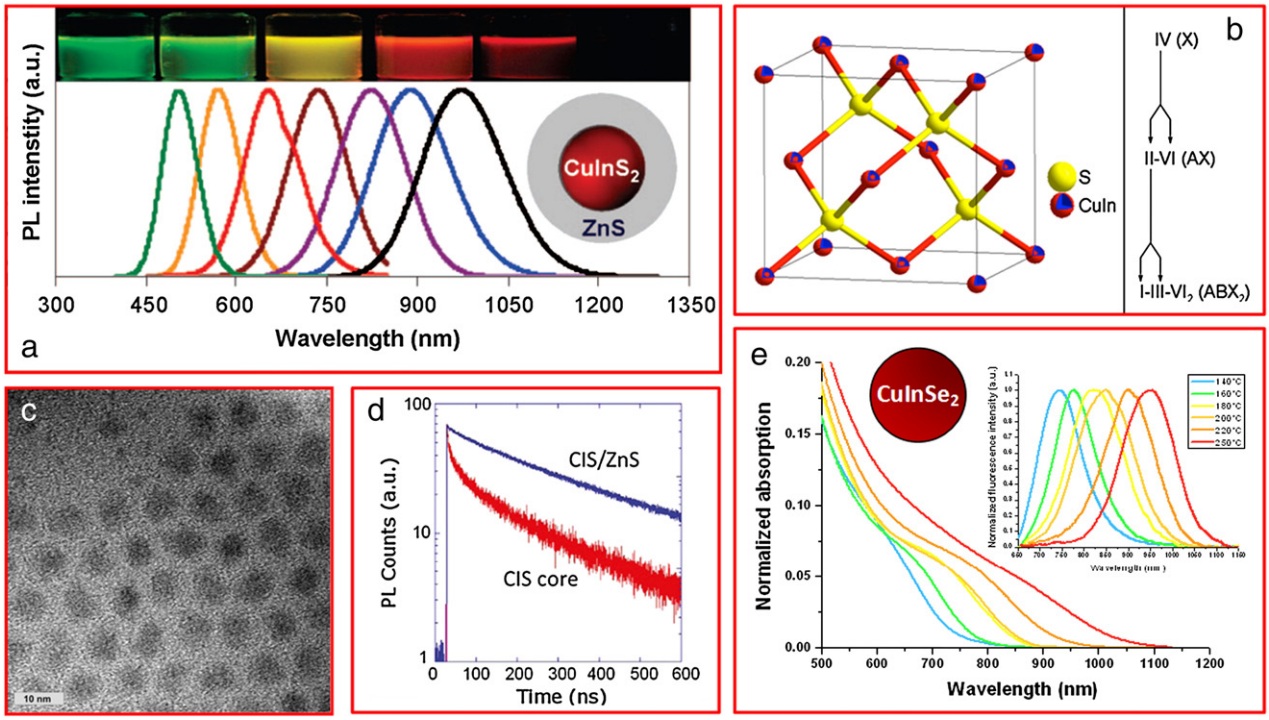

Fig. 2. a) Photoluminescence properties of $CuInS_2$/ZnS core/shell NCs [80]; b) Left: Crystal structure of zinc blende $CuInS_2$ NCs; right: schematic relationship among group IV, II–VI and I–III–VI_2 semiconductor materials [85,167]; c) TEM image of $CuInS_2$/ZnS NCs [36]; d) PL decay of $CuInS_2$ core and $CuInS_2$/ZnS core/shell NCs [88]; e) Absorption (inset: PL) spectra of Cu–In–Se core NCs [37].
Reprinted with permission from American Chemical Society copyright (2008, 2009, 2010, 2011) and American Institute of Physics copyright (2009).

the whole NIR window, good quantum yields (>30%), size below 10 nm, and lifetimes in the range of few hundreds of ns. Recent works tend to focus on the synthesis of NIR QDs that do not contain toxic compounds. This effort is necessary if such probes are to be used *in vivo*, and has to be combined with the effort to fine tune the QD surface chemistry with various organic molecules so that QDs can be as furtive as possible, reach their target efficiently, and/or be excreted.

2.8. Quick overview of QD surface chemistry

Most QD synthesis schemes are performed in organic solvents. QDs are then capped with hydrophobic ligands usually consisting of an anchoring group and one or more aliphatic chains. These QDs must therefore be modified to become soluble in water and compatible with the biological environment. The QD surface chemistry determines its final size, colloidal stability, charge, non specific adsorption and specific affinity and as such has a strong influence on its interaction with its environment and, *in fine*, on its *in vivo* biodistribution. The aim of this paragraph is not to present a comprehensive review of the different QD surface chemistry used for *in vivo* imaging, but to give a quick and general overview of the main strategies used to solubilize QDs in water. The reader may refer to several excellent reviews for more detailed information on QD solubilization and conjugation with biomolecules [92–94]. Most solubilization techniques can be classified into two general schemes applicable to many types of nanoparticles: encapsulation and cap-exchange. Encapsulation consists in keeping the initial hydrophobic ligands and surrounding the QD with amphiphilic molecules, with hydrophobic chains interdigitating with the QD ligands and hydrophilic groups for water solubilization. Popular examples of amphiphilic molecules are phospholipid micelles or amphiphilic copolymers [93,95,96]. In contrast, cap-exchange consists in replacing the hydrophobic ligands with new ligands presenting anchoring groups to bind to the nanocrystal surface and hydrophilic solubilizing groups. Anchoring groups may be composed of phosphines [97], amines, carboxylates, and most commonly thiols or di-thiols [98–101]. Hydrophilic groups used in these two strategies may be composed of charged moieties (carboxylic acids, amines…), however these present limited stability and high non specific adsorption of biomolecules on their surface. Polyethylene glycol (PEG) chains are more common for *in vivo* applications as it decreases considerably this non specific adsorption, at the cost of an increased size [95,96,98,99]. Zwiterrions present an interesting alternative to PEG, as they also allow a low non specific adsorption level while maintaining a small overall hydrodynamic size [100,101]. Finally, other strategies include growth of (<20 nm) silica shells [102,103] and encapsulation in or deposition at the surface of larger (100 nm–μm) colloids (polymer or silica beads, liposomes…) [104,105]. Every *in vivo* imaging application presents different requirements in terms of size, charge, specific and non specific adsorption levels… As a consequence, the universal optimal surface chemistry does not exist. Instead, the QD surface chemistry should be tailored according to the specific criteria of each imaging application, as will be discussed in the next sections.

3. *In vivo* imaging applications

Visible emitting QDs have initially been used for cellular imaging, to label and track specific molecular targets in live or fixed cultured cell samples [92,95,106]. They have then been used as *in vivo* markers in small organisms, for example to study cell lineage in early stage *Xenopus* embryos [96]. Visible emitting QDs are well adapted to these thin and transparent samples. They however provide poor signal-to-background ratio in thicker tissue sections and when imaging targets in small animals due to the tissue absorption and diffusion, and to the strong auto-fluorescence background from endogenous chromophores in the visible region. Near infrared emitting QDs thus allow much more sensitive detection of deeper targets, up to several centimeters below the surface. These characteristics triggered the development of many *in vivo* imaging applications. We will briefly describe some of these in the following sections and discuss the influence of QD design on each specific application, including lymph and blood vasculature imaging and tumor detection. We will then describe other developments of NIR emitting QDs associated with cell tracking and multimodal probes that combine the QD fluorescence with a whole body imaging contrast, such as magnetic resonance imaging (MRI) or positron emission tomography (PET).

3.1. Lymph node imaging

The sentinel lymph node (SLN) is the first regional step of lymphatic drainage and metastasis of the primary tumor. In the treatment of breast cancer, the axillary lymph node status is the major prognostic factor and a determinant predictor of recurrence and survival [107]. As the current method for the detection of SLN presents some disadvantages such as allergic reaction to blue dye, the use of radioactive tracers and long hospitalization, the use of fluorescence to localize the SLN has been developed since several years.

The first near-infrared emitting fluorophore used in the detection of the SLN was indocyanine green (ICG). First *in vivo* reports [108] demonstrated the aggregation of ICG and its release from SLN, both effects related to the small size of the molecule. Fast photobleaching is another critical issue that considerably diminishes the feasibility of ICG-based fluorescence imaging of organs. QDs, due to their resistance to photobleaching and their hydrodynamic diameter, which may be tuned in function of core size and surface chemistry, offer interesting opportunities for SLN infrared imaging.

Several studies on the detection of SLN using near infrared emitting QD have been reported and are summarized in Table S1. The initial papers studying the SLN mapping *in vivo* using NIR emitting QDs have been reported by Frangioni's team. The authors have used CdTe/CdSe core/shell QDs to visualize axillary lymph nodes as deep as 1 cm from the skin surface either after a subcutaneous injection in the paw of healthy mice, or after intradermal injection on the thigh of pig [109] or in the model of spontaneous melanoma of Sinclair mini-swine [110]. The superficial lymph node could be detected through the skin but to map deeper SLN like those from pleural space [111], esophagus [112] or gastrointestinal tract [113], the rib cage or the abdominal cavity of the Yorkshire pigs was opened. Another formulation of QDs with a core composed of indium and arsenic has shown a good SLN mapping in mice and rats [114] but the size of QDs should be controlled so that QDs do not migrate to the surrounding tissue or further into the lymphatic system.

Indeed, the size of the nanoparticles is crucial to SLN mapping because nanoparticles too small (<10 nm) can flow through the SLN and diffuse in surrounding tissue or in other lymph nodes in the chain whereas nanoparticles too large do not migrate and stay at the injection point [115]. Charge and nature of the QD surface chemistry do not seem to directly influence the capture of intra-tumorally or subcutaneously injected QDs by the SLNs, even though charge plays a crucial role for serum protein adsorption, which may increase the size of QD–protein corona assembly and therefore its retention in the SLN. SLN mapping, in that respect, is much easier than tumor or organ targeting after intravenous injection (see below) [116,117].

The major obstacle to the QDs clinical translation is their toxicity. The QD core is often composed of heavy metals (Cd, Te, Se or As), which could be released in the body due to the QD degradation and oxidation. In our recent studies [35,118], we have compared the detection of SLN and the toxicity of two types of QDs in a model of healthy mice. Both QD types, CdTeSe/CdZnS and $CuInS_2$/ZnS QDs, allow the localization of the axillary lymph node in few minutes after subcutaneous injection (20 pmol) (Fig. 3). Unlike cadmium-QDs, which demonstrated the clear features of local toxicity, such as an increased lymph node weight with several inflammatory areas, the indium-based QDs

did not show any signs of toxicity upon the same experimental conditions. Moreover, the inflammation threshold corresponded to a fifty time higher concentration of $CuInS_2$/ZnS compared to CdTeSe/CdZnS QDs.

Silicon QDs are also of particular interest because of their biocompatible composition and tunable emission properties in function of particle size. These Si QDs, whose hydrodynamic diameter is 20 nm, migrate to the SLN after subcutaneous injection in mice and no sign of toxicity (mice behavior, histopathology analysis of major organs and blood parameters) has been observed, clearly indicating the biocompatibility of these nanoparticles [46]. However, the inability to excite these QDs in the NIR range strongly limits the attainable imaging depth.

SLN detection using most of these QDs only takes a few minutes after injection, which greatly simplifies surgical procedures. The QDs then slowly leak from the injection point and the SLN into the rest of the organism via blood and lymph circulation [118]. This provides a window of a few hours for the surgeon to resect both the SLN and the injection point, removing at the same time the large majority of the injected QDs from the body and limiting toxicity issues. Ideally, the small amount of QDs remaining in the body after the operation should be ultimately eliminated, either via the kidneys into the urine or via the hepatobiliary pathway. The mechanisms for complete clearance are however not well understood yet.

3.2. Vasculature imaging; renal elimination vs. sequestration

The biodistribution of QDs after intravenous injection is strongly dependent on their surface chemistry. In general, QDs distribute rapidly in the entire bloodstream, allowing direct visualization of blood vasculature. Naturally, small capillaries are only spatially resolved close to the surface due to diffusion of light by the surrounding tissues, while larger vessels may be imaged deeper. Larson et al. used two-photon excitation microscopy to image blood circulation in the ear of a mouse with final QD concentration in the blood on the order of 1 μM [16]. In this concentration regime, erythrocytes can be detected as dark volumes flowing through an otherwise uniformly fluorescent blood vessel. They were thus able to measure changes in local flow velocities. Smith et al. demonstrated the use of QDs to image chick embryo chorioallantoic membrane vasculature, a model test system for blood vessel formation and development [119]. While visible emitting QDs offered a poor contrast, NIR QDs led to a drastic improvement of signal-to-noise ratio due to the low auto-fluorescence background in this spectral region. Blood vessels could be imaged on multiple scales, from large vessels at the whole embryo level to small capillaries. In both studies, QDs were beneficial compared to fluorescein-labeled dextrans, a common angiogenic imaging probe, due to their higher brightness and to their emission in the more favorable NIR region.

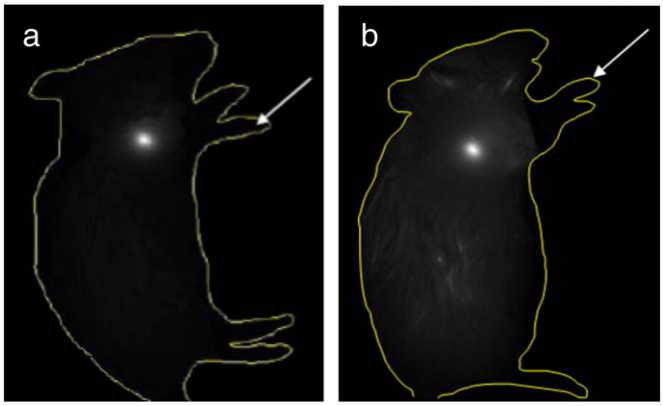

Fig. 3. *In vivo* fluorescence imaging of the right axillary lymph node of mice with Fluobeam® 5 min after subcutaneous injection of 20 pmol of CdTeSe/CdZnS (a) or $CuInS_2$/ZnS (b) QDs in the right anterior paw. The exposure time is 10 ms (a) or 50 ms (b) and the injection point (white arrow) was hidden.

After some time in the bloodstream, QDs are eliminated from the body or sequestrated in one or several organs. Elimination via the kidneys into the bladder requires very small hydrodynamic sizes. A threshold of 5.5 nm in hydrodynamic diameter was for example found for cysteine-capped QDs [25]. Since NIR emitting QDs are usually larger than this, they tend to remain in the body. Their biodistribution kinetics and final repartition strongly depend on their surface chemistry. Most types of QDs become opsonized in the circulation and are captured by macrophages in organs of the reticuloendothelial system (RES) (liver, spleen, bone marrow, lymph nodes…) [120–122]. QD circulation times are thus determined by how long they are able to evade opsonization. Functionalizing QDs with larger PEG (molecular weight larger than 2000 g/mol) chains thus prolongs circulation times, as has been shown with a variety of nanoparticles [123] but do not avoid final capture by the RES [120,124]. On the other hand, QDs capped with smaller PEG ligands seem to display a strongly size-dependent biodistribution. Choi et al. tested small InAs/ZnS QDs capped with smaller PEG ligands (MW ranging from 100 to 1000 g/mol) [39]. While very short (<100 g/mol) PEG chains proved inefficient in evading opsonization, short (typ. 200 g/mol) PEG chains allowed QD elimination into the urine. Functionalization with longer PEG chains led to an increase in hydrodynamic size, preventing filtration by the kidneys and finally leading to accumulation in RES and other organs in a size-dependent manner. PEG length is however probably not the only determinant of QD biodistribution, but certainly PEG density and stability of the surface chemistry on the QD surface must also strongly influence the fate of QD after intravenous injection. The mechanism and optimal conditions for final excretion of QDs via the hepatobiliary pathway remain unclear. In particular, most QDs seem to remain sequestrated in the liver for long periods of time, up to two years after injection [125]. In contrast, a recent study provided evidence for renal and hepatobiliary excretion of silica-coated CdSe QDs, for which elimination was completed by 120 h [126].

3.3. Tumor imaging

In vivo fluorescence imaging of tumors using NIR QDs is a very active area of research as it may provide tools to locate tumors and metastases or map tumor margins during surgery. Indeed, surgical removal of a tumor is often the best method of cure for cancer. Incomplete resection of a neoplasm is a major factor that compromises the long-term survival rate of cancer patients. Adequate assessment of the extent of the disease is limited during surgery because it relies on palpation and visual inspection. The effect is in a 40–80% recurrence rate, like in retroperitoneal sarcoma, brain or breast neoplasms [127,128]. Surgeons are required to remove large surgical margins around what they perceive as a neoplastic tissue because of the microscopic tumoral dissemination in the surrounding healthy tissues. It is therefore important to develop new technologies that will help achieve precise delineation of tumor margins and improved visibility of small tumors that are difficult to distinguish from normal tissues. Fluorescence-guided surgery using NIR emitting nanoparticles is an emerging technology that holds potential to provide a viable solution to this problem, and as a consequence several strategies are being developed to target QDs to tumoral cells *in vivo*.

Many types of circulating nanoparticles have been shown to accumulate in the tumor due to leaky blood vessels and inefficient lymphatic drainage [129,130]. This effect is known as enhanced permeation and retention (EPR) effect, and was also verified with QDs in several studies (Fig. 4a,b) [131,132]. The shape and size of the nanoprobes play a crucial role in this process, since smaller particles seem to penetrate deeper

into the tumor interstitial medium [133]. Similarly, for a given nanoparticle volume, rod-shaped QDs seem to provide more efficient labeling than spherical ones [134]. On the other hand, small particles are more likely to be washed out of the tumor [135], and the optimal nanoparticle size likely depends on the imaging parameters (e.g. delay between injection and imaging) and the type of tumor. However the level of EPR-mediated QD tumor capture is often low, and is unlikely to allow efficient detection of micrometastases.

Several methods have thus been proposed to design targeted QDs and increase their specific uptake efficiency. In general, intravenously injected QDs must meet several criteria to efficiently label their target: long circulation times for prolonged exposure to the target, slow clearance from the bloodstream by the RES and strong affinity for their target for fast binding and minimal release back into the blood or lymph circulation. Most of these QDs are therefore coated with long chain PEG for minimization of non specific adsorption and prolonged circulation and further conjugated with targeting moieties. While functional QDs have been successfully targeted to different tissues, such as blood or lymphatic vessel [136–138] liver, [139] or lung [136], there is an important effort toward the design of efficient tumor-targeting QDs. QDs conjugated with antibodies against tumor-specific antigens were for example shown to label tumors xenografted in mice much more efficiently than non-targeted QDs [131,140–142]. Tada et al. have tracked the path and kinetics of diffusion of single QDs targeted to the human endothelial growth factor 2 (HER2) into the targeted tumor (Fig. 4c) [141]. They were able to show that the QD first circulates into blood vessels, then extravasates from the vessel into the tumor extracellular space and binds its HER2 target at a tumoral cell membrane before getting internalized and transported to the perinuclear region. QDs conjugated to the endothelial growth factor (EGF) have also been shown to efficiently target HER2 both *in vitro* [143] on cultured cells and *in vivo* to label tumors [144]. Another popular strategy relies on the RGD peptide sequence to target QDs to integrin $\alpha_v\beta_3$, a receptor involved in angiogenesis, proliferation and metastasis, which is upregulated in certain tumor types [46,145–147]. Again, targeted QDs showed higher uptake efficiency compared to non-targeted ones in tumor-bearing mice. The small size of RGD sequences allowed binding of multiple targeting peptides to the QDs and increased their global affinity for integrins. Imaging of tumor frozen sections and real-time intravital RGD-QDs tracking showed that these QDs did not extravasate but indeed bound to the tumor vessel walls [145,146]. Interestingly, the authors observed that RGD-QDs bound to their specific integrin targets majoritarily as small aggregates and not as single nanoparticles [146]. These aggregates were also able to transiently bind to vessel walls in non-tumoral tissues but were rapidly washed back into the bloodstream. This effect is not completely understood yet but was tentatively attributed to the laminar flow in blood vessels and to polyvalent binding of QD aggregates to several molecular targets on the cell surface.

This emphasizes the influence of the nanoparticle size on its biodistribution and its targeting efficiency. Larger particles (100 nm–few μm) may therefore be preferable for specific imaging or drug delivery applications. QDs have thus been incorporated into immunoliposomes, silica beads or polymer nanoparticles to provide them with a good NIR fluorescence contrast [133,148–150]. For example Weng et al. have used 100 nm diameter liposomes as a nano-platform with drugs inside and NIR fluorescent QDs and tumor-targeting antibody fragments on the surface [149]. QDs allowed visualization of the liposome uptake into tumors xenografted in mice. Similar constructs could be used to combine diagnostics and therapeutic abilities, for example to follow where drugs are being delivered during the treatment.

3.4. Cell tracking

Cell tracking using NIR fluorescent QDs is also a very active and promising area of research. The ability to track tumoral, stem, or immune cells *in vivo* after injection is central to many biological studies. QDs have thus been used to label these cells *in vitro*, either by labeling specific membrane receptors or by endocytosis. QD-labeled cells are then injected *in vivo* and their biodistribution can be mapped using the QD fluorescence signal (Fig. 5) [151–156]. For these studies,

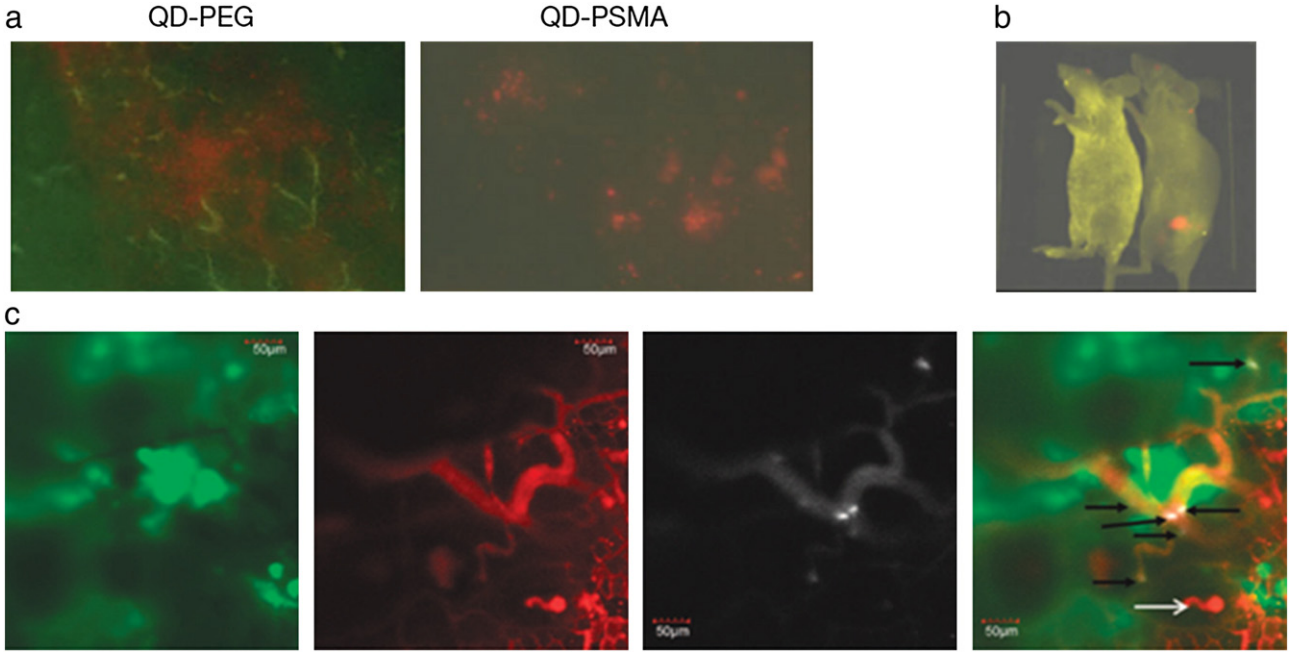

Fig. 4. a) Histological examination of QD uptake in C4-2 tumor xenografts maintained in athymic nude mice by EPR effect (QD PEG) or active antibody-mediated targeting (QD PSMA). b) *In vivo* tumor imaging of in live mice using antibody-targeted QDs. Colors correspond to spectrally unmixed fluorescence signals from the autofluorescence (yellow) and QDs (red) [131]. c) Direct visualization of binding of RGD-QD to tumor vessel endothelium. From left to right: green channel shows EGFP-expressing cancer cells, while the red channel outlines the tumor's vasculature via injection of Angiosense dye. The NIR channel shows intravascularly administered QDs which remain in the vessels and do not extravasate. QD binding events are marked by black arrows in the merge image [146].
Reprinted with permission from Macmillan Publishers Ltd: Nature Biotechnology copyright (2004) and with permission from American Chemical Society copyright (2008).

suitable QDs should be able to efficiently label target cells *in vitro* and more importantly they should not leave these cells after the *in vivo* injection, to maintain a perfect correspondence between the injected cell biodistribution and the QD fluorescence signal. In several studies, QDs were shown to remain inside their initial cells during the experiment, from a few hours up to four weeks *in vivo* [153]. The ability to easily separate fluorescence from different QD populations allows imaging the migration of several cell types simultaneously and studying their interactions *in vivo* [152]. Near infrared QDs enhance the imaging sensitivity over visible emitting fluorophores, enabling detection of only 5000 cells subcutaneously [155].

3.5. Multimodal QDs

Near infrared fluorescence imaging is flexible, cheap, easy to use and sensitive; however it is limited to depths of a few centimeters below the skin. In contrast, magnetic resonance imaging (MRI), scintigraphy, single photon emission computed tomography (SPECT) and positron emission tomography (PET) give access to whole-body images, with smaller spatial resolution. There is therefore a large interest in combining fluorescence with another imaging modality to benefit from the advantages of the two techniques. Quantum dots constitute in this regard promising platforms to assemble different contrast agents to form multimodal nanoprobes. Several examples of QD-based multimodal probes have been described in the literature, including MRI/fluorescence and PET/fluorescence probes [157]. One of the most common strategy used to build these probes consists in coating the QDs or conjugating them with paramagnetic (for MRI) or radioactive (for PET) ion chelates or molecules. For example, Mulder et al. incorporated a Gd-chelating lipid into QD phospholipid micelles [158,159]. The micelle was further functionalized by conjugation with targeting RGD-peptides. This probe enabled visualization of angiogenesis regions by MRI and visualization of the tumor blood vessels with a higher resolution using fluorescence. In another application, Duconge et al. designed ^{18}F-labeled QD micelles; this dual PET-fluorescence probe was injected in the tail vein of a mouse [121]. These enabled to quantitatively measure the whole-body QD biodistribution in real-time using PET and pharmacokinetic parameters such as blood circulation time. Fluorescence images were then obtained by fluorescence confocal endoscopy to image the QD distribution at the intracellular level.

Another strategy to build multimodal probe is the doping of QDs with paramagnetic ions such as Mn. This has been demonstrated using different types of QDs, including CdSe, CdS, CdTe, or Si-based nanocrystals [157]. Wang et al. synthesized visible emitting CdSe/$Zn_{(1-x)}Mn_xS$ water soluble QDs and internalized them into cultured cells [160]. These QDs produced sufficient contrast to allow visualization of the cells using both MRI and fluorescence microscopy. The same strategy was used with NIR emitting CdTeSe/CdS QDs however bimodal imaging has not been demonstrated *in vivo* yet [161]. Finally, a third strategy consists in assembling QDs with Fe_3O_4 or FePt magnetic nanoparticles in silica beads, micelles, polymer particles, or within nano-heterostructures (nanoparticles composed of a magnetic part and a semiconducting part) [162–165].

4. Conclusion and perspectives

Recent years have witnessed the development of bright near infrared emitting QDs of different sizes, compositions and properties. This allows tailoring the choice of the NIR probe depending on the application and the desired properties. The available NIR QDs offer a wide range of emission wavelengths spanning the optical window for deep tissue imaging, lifetimes ranging from a few tens to a few hundred nanoseconds, compositions presenting limited toxicity… The type of surface chemistry may also be chosen from a variety of different solubilization strategies, some of which enable renal elimination of small QDs, other long circulation times and further conjugation of targeting molecules. This has permitted the development of several *in vivo* imaging applications, relying on simple QD diffusion (lymph node mapping, vasculature imaging…) or more complex targeted imaging of tumoral cells. Currently available near infrared QDs therefore represent a powerful tool for *in*

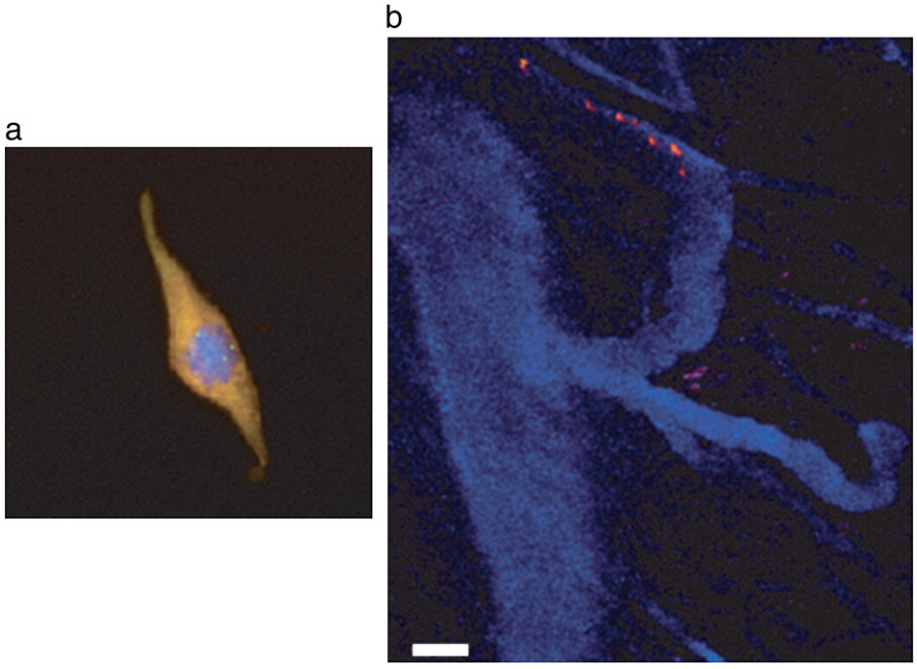

Fig. 5. Cell labeling and tracking using endocytosed QDs. a) Single cell labeled with QDs before *in vivo* injection. b) Seven images superimposed in time as a single bone marrow lineage-negative cell labeled with QD590-TAT (orange) navigated the tumor vessels highlighted with QD470 micelles (blue) *in vivo*. Scale bar is 50 μm.
Reprinted by permission from Macmillan Publishers Ltd: Nature Medicine, [156] copyright (2005).

vivo biological studies, and we expect that they will become increasingly used in many studies such as cell tracking, tumor imaging, drug screening…

Fluorescence imaging holds great promises to assist oncological surgery due to simple incorporation to surgical inspection to delineate tumor margins or map sentinel lymph nodes [166]. The detection sensitivity of these techniques suffers from the lack of high brightness/high stability organic fluorophores emitting in the NIR. In that respect, QDs have the potential to significantly improve the performance of near infrared fluorescence imaging for optically assisted surgery thanks to their superior optical characteristics compared to organic dyes. However two main challenges still need to be resolved before this technique can reach the clinical field. First, efficient targeting strategies must be developed to ensure sensitive labeling of very small metastases. *In vivo* targeting is a more global scientific and biotechnological problem that is shared with many other biotechnological fields, in imaging and drug delivery. Steady progress in targeting efficiency is being made, and we can expect satisfying results in the near to mid future. Second, if QDs are to be used in clinical applications, there should be no reasonable doubt about short and long term toxicity. This implies the development of QDs with minimal toxicity, which has already begun but can certainly progress further, and the elimination of injected QDs from the body, which is currently less advanced. While some sufficiently small particles with specific surface chemistries may present a certain degree of renal elimination, complete elimination will probably require either degradation into smaller atomic components and/or nanoparticles that are efficiently eliminated from RES organs into the bile and the intestines.

Supplementary data to this article can be found online at http://dx.doi.org/10.1016/j.addr.2012.08.016.

References

[1] Y.T. Lim, S. Kim, A. Nakayama, N.E. Stott, M.G. Bawendi, J.V. Frangioni, Selection of quantum dot wavelength for biomedical assays and imaging, Mol. Imaging 2 (2003) 50–64.
[2] A.M. Smith, M.C. Mancini, S.M. Nie, Second window for in vivo imaging, Nat. Nanotechnol. 4 (2009) 710–711.
[3] V.J. Pansare, S. Hejazi, W.J. Faenza, R.K. Prud'homme, Review of long-wavelength optical and NIR imaging materials: contrast agents, fluorophores, and multifunctional nano carriers, Chem. Mater. 24 (2012) 812–827.
[4] P.C.N. Rensen, R.L.A. de Vrueh, J. Kuiper, M.K. Bijsterbosch, E.A.L. Biessen, T.J.C. van Berkel, Recombinant lipoproteins: lipoprotein-like lipid particles for drug targeting, Adv. Drug Deliv. Rev. 47 (2001) 251–276.
[5] B.M. Barth, E.I. Altinoglu, S.S. Shanmugavelandy, J.M. Kaiser, D. Crespo-Gonzalez, N.A. DiVittore, C. McGovern, T.M. Goff, N.R. Keasey, J.H. Adair, T.P. Loughran, D.F. Claxton, M. Kester, Targeted indocyanine-green-loaded calcium phosphosilicate nanoparticles for in vivo photodynamic therapy of leukemia, ACS Nano 5 (2011) 5325–5337.
[6] M. Kester, Y. Heakal, T. Fox, A. Sharma, G.P. Robertson, T.T. Morgan, E.I. Altinoglu, A. Tabakovic, M.R. Parette, S.M. Rouse, V. Ruiz-Velasco, J.H. Adair, Calcium phosphate nanocomposite particles for in vitro imaging and encapsulated chemotherapeutic drug delivery to cancer cells, Nano Lett. 8 (2008) 4116–4121.
[7] H.S. Muddana, T.T. Morgan, J.H. Adair, P.J. Butler, Photophysics of Cy3-encapsulated calcium phosphate nanoparticles, Nano Lett. 9 (2009) 1559–1566.
[8] J.F. Bringley, T.L. Penner, R.Z. Wang, J.F. Harder, W.J. Harrison, L. Buonemani, Silica nanoparticles encapsulating near-infrared emissive cyanine dyes, J. Colloid Interface Sci. 320 (2008) 132–139.
[9] D. Knopp, D.P. Tang, R. Niessner, Bioanalytical applications of biomolecule-functionalized nanometer-sized doped silica particles, Anal. Chim. Acta 647 (2009) 14–30.
[10] X.H. Wang, A.R. Morales, T. Urakami, L.F. Zhang, M.V. Bondar, M. Komatsu, K.D. Belfield, Folate receptor-targeted aggregation-enhanced near-IR emitting silica nanoprobe for one-photon in vivo and two-photon ex vivo fluorescence bioimaging, Bioconjug. Chem. 22 (2011) 1438–1450.
[11] M. Pelton, J. Aizpurua, G. Bryant, Metal-nanoparticle plasmonics, Laser Photonics Rev. 2 (2008) 136–159.
[12] L.R. Hirsch, A.M. Gobin, A.R. Lowery, F. Tam, R.A. Drezek, N.J. Halas, J.L. West, Metal nanoshells, Ann. Biomed. Eng. 34 (2006) 15–22.
[13] X. Yuan, Z. Luo, Q. Zhang, X. Zhang, Y. Zheng, J.Y. Lee, J. Xie, Synthesis of Highly Fluorescent Metal (Ag, Au, Pt, and Cu) Nanoclusters by Electrostatically Induced Reversible Phase Transfer, ACS Nano 5 (2011) 8800–8808.
[14] A.M. Smith, A.M. Mohs, S. Nie, Tuning the optical and electronic properties of colloidal nanocrystals by lattice strain, Nat. Nanotechnol. 4 (2009) 56–63.
[15] H. Mattoussi, G. Palui, H.B. Na, Luminescent quantum dots as platforms for probing in vitro and in vivo biological processes, Adv. Drug Deliv. Rev. 64 (2012) 138–166.
[16] D.R. Larson, W.R. Zipfel, R.M. Williams, S.W. Clark, M.P. Bruchez, F.W. Wise, W.W. Webb, Water-soluble quantum dots for multiphoton fluorescence imaging in vivo, Science 300 (2003) 1434–1436.
[17] F. Helmchen, W. Denk, Deep tissue two-photon microscopy, Nat. Methods 2 (2005) 932–940.
[18] S.W. Wu, G. Han, D.J. Milliron, S. Aloni, V. Altoe, D.V. Talapin, B.E. Cohen, P.J. Schuck, Non-blinking and photostable upconverted luminescence from single lanthanide-doped nanocrystals, Proc. Natl. Acad. Sci. U. S. A. 106 (2009) 10917–10921.
[19] M.K. So, C.J. Xu, A.M. Loening, S.S. Gambhir, J.H. Rao, Self-illuminating quantum dot conjugates for in vivo imaging, Nat. Biotechnol. 24 (2006) 339–343.
[20] Q.L. de Chermont, C. Chaneac, J. Seguin, F. Pelle, S. Maitrejean, J.P. Jolivet, D. Gourier, M. Bessodes, D. Scherman, Nanoprobes with near-infrared persistent luminescence for in vivo imaging, Proc. Natl. Acad. Sci. U. S. A. 104 (2007) 9266–9271.
[21] E.I. Altinoglu, J.H. Adair, Near infrared imaging with nanoparticles, Wiley Interdiscip. Rev. Nanomed. Nanobiotechnol. 2 (2010) 461–477.
[22] R.G. Aswathy, Y. Yoshida, T. Maekawa, D.S. Kumar, Near-infrared quantum dots for deep tissue imaging, Anal. Bioanal. Chem. 397 (2010) 1417–1435.
[23] X.X. He, K.M. Wang, Z. Cheng, In vivo near-infrared fluorescence imaging of cancer with nanoparticle-based probes, Wiley Interdiscip. Rev. Nanomed. Nanobiotechnol. 2 (2010) 349–366.
[24] Q.A. Ma, X.G. Su, Near-infrared quantum dots: synthesis, functionalization and analytical applications, Analyst 135 (2010) 1867–1877.
[25] H.S. Choi, W. Liu, P. Misra, E. Tanaka, J.P. Zimmer, B.I. Ipe, M.G. Bawendi, J.V. Frangioni, Renal clearance of quantum dots, Nat. Biotechnol. 25 (2007) 1165–1170.
[26] D.E. Gomez, J. van Embden, P. Mulvaney, M.J. Fernee, H. Rubinsztein-Dunlop, Exciton-trion transitions in single CdSe–CdS core–shell nanocrystals, ACS Nano 3 (2009) 2281–2287.
[27] M.A. Hines, P. Guyot-Sionnest, Synthesis and characterization of strongly luminescing ZnS-capped CdSe nanocrystals, J. Phys. Chem. 100 (1996) 468–471.
[28] S. Ithurria, P. Guyot-Sionnest, B. Mahler, B. Dubertret, Mn(2+) as a radial pressure gauge in colloidal core/shell nanocrystals, Phys. Rev. Lett. 99 (2007).
[29] O. Faklaris, V. Joshi, T. Irinopoulou, P. Tauc, M. Sennour, H. Girard, C. Gesset, J.C. Arnault, A. Thorel, J.P. Boudou, P.A. Curmi, F. Treussart, Photoluminescent diamond nanoparticles for cell labeling: study of the uptake mechanism in mammalian cells, ACS Nano 3 (2009) 3955–3962.
[30] F. Erogbogbo, C.A. Tien, C.W. Chang, K.T. Yong, W.C. Law, H. Ding, I. Roy, M.T. Swihart, P.N. Prasad, Bioconjugation of luminescent silicon quantum dots for selective uptake by cancer cells, Bioconjug. Chem. 22 (2011) 1081–1088.
[31] T. Pons, N. Lequeux, B. Mahler, S. Sasnouski, A. Fragola, B. Dubertret, Synthesis of near-infrared-emitting, water-soluble CdTeSe/CdZnS core/shell quantum dots, Chem. Mater. 21 (2009) 1418–1424.
[32] B. Blackman, D. Battaglia, X.G. Peng, Bright and water-soluble near IR-emitting CdSe/CdTe/ZnSe Type-II/Type-I nanocrystals, tuning the efficiency and stability by growth, Chem. Mater. 20 (2008) 4847–4853.
[33] Z. Deng, O. Schulz, S. Lin, B. Ding, X. Liu, X. Wei, R. Ros, H. Yan, Y. Liu, Aqueous synthesis of zinc blende CdTe/CdS magic-core/thick-shell tetrahedral-shaped nanocrystals with emission tunable to near-infrared, J. Am. Chem. Soc. 132 (2010) 5592–5593.
[34] S. Kim, B. Fisher, H.J. Eisler, M. Bawendi, Type-II quantum dots: CdTe/CdSe(core/shell) and CdSe/ZinTe(core/shell) heterostructures, J. Am. Chem. Soc. 125 (2003) 11466–11467.
[35] T. Pons, E. Pic, N. Lequeux, E. Cassette, L. Bezdetnaya, F. Guillemin, F. Marchal, B. Dubertret, Cadmium-free CuInS(2)/ZnS quantum dots for sentinel lymph node imaging with reduced toxicity, ACS Nano 4 (2010) 2531–2538.
[36] L. Li, T.J. Daou, I. Texier, T.T. Kim Chi, N.Q. Liem, P. Reiss, Highly luminescent CuInS2/ZnS core/shell nanocrystals: cadmium-free quantum dots for in vivo imaging, Chem. Mater. 21 (2009) 2422–2429.
[37] E. Cassette, T. Pons, C. Bouet, M. Helle, L. Bezdetnaya, F. Marchal, B. Dubertret, Synthesis and characterization of near-infrared Cu–In–Se/ZnS core/shell quantum dots for in vivo imaging, Chem. Mater. 22 (2010) 6117–6124.
[38] P.M. Allen, W.H. Liu, V.P. Chauhan, J. Lee, A.Y. Ting, D. Fukumura, R.K. Jain, M.G. Bawendi, InAs(ZnCdS) quantum dots optimized for biological imaging in the near-infrared, J. Am. Chem. Soc. 132 (2010) 470–471.
[39] H.S. Choi, B.I. Ipe, P. Misra, J.H. Lee, M.G. Bawendi, J.V. Frangioni, Tissue- and organ-selective biodistribution of NIR fluorescent quantum dots, Nano Lett. 9 (2009) 2354–2359.
[40] S. Tamang, G. Beaune, I. Texier, P. Reiss, Aqueous Phase Transfer of InP/ZnS Nanocrystals Conserving Fluorescence and High Colloidal Stability, ACS Nano 5 (2011) 9392–9402.
[41] H.G. Zhao, D.F. Wang, T. Zhang, M. Chaker, D.L. Ma, Two-step synthesis of high-quality water-soluble near-infrared emitting quantum dots via amphiphilic polymers, Chem. Commun. 46 (2010) 5301–5303.
[42] J.Y. Fan, P.K. Chu, Group IV nanoparticles: synthesis, properties, and biological applications, Small 6 (2010) 2080–2098.
[43] E.H. Sargent, Infrared quantum dots, Adv. Mater. 17 (2005) 515–522.
[44] L. Mangolini, D. Jurbergs, E. Rogojina, U. Kortshagen, High efficiency photoluminescence from silicon nanocrystals prepared by plasma synthesis and organic surface passivation, Phys. Status Solidi C 3 (2006) 3975–3978.
[45] L. Mangolini, E. Thimsen, U. Kortshagen, High-yield plasma synthesis of luminescent silicon nanocrystals, Nano Lett. 5 (2005) 655–659.
[46] F. Erogbogbo, K.T. Yong, I. Roy, R. Hu, W.C. Law, W.W. Zhao, H. Ding, F. Wu, R. Kumar, M.T. Swihart, P.N. Prasad, In vivo targeted cancer imaging, sentinel lymph node mapping and multi-channel imaging with biocompatible silicon nanocrystals, ACS Nano 5 (2011) 413–423.
[47] Y. He, Y.L. Zhong, F. Peng, X.P. Wei, Y.Y. Su, Y.M. Lu, S. Su, W. Gu, L.S. Liao, S.T. Lee, One-pot microwave synthesis of water-dispersible, ultraphoto- and pH-stable, and highly fluorescent silicon quantum dots, J. Am. Chem. Soc. 133 (2011) 14192–14195.

[48] J.H. Park, L. Gu, G. von Maltzahn, E. Ruoslahti, S.N. Bhatia, M.J. Sailor, Biodegradable luminescent porous silicon nanoparticles for in vivo applications, Nat. Mater. 8 (2009) 331–336.
[49] D.C. Lee, J.M. Pietryga, I. Robel, D.J. Werder, R.D. Schaller, V.I. Klimov, Colloidal synthesis of infrared-emitting germanium nanocrystals, J. Am. Chem. Soc. 131 (2009) 3436–3437.
[50] D.A. Ruddy, J.C. Johnson, E.R. Smith, N.R. Neale, Size and bandgap control in the solution-phase synthesis of near-infrared-emitting germanium nanocrystals, ACS Nano 4 (2010) 7459–7466.
[51] E.J. Henderson, M. Seino, D.P. Puzzo, G.A. Ozin, Colloidally stable germanium nanocrystals for photonic applications, ACS Nano 4 (2010) 7683–7691.
[52] J.R. Rabeau, Y.L. Chin, S. Prawer, F. Jelezko, T. Gaebel, J. Wrachtrup, Fabrication of single nickel-nitrogen defects in diamond by chemical vapor deposition, Appl. Phys. Lett. 86 (2005).
[53] I.I. Vlasov, A.S. Barnard, V.G. Ralchenko, O.I. Lebedev, M.V. Kanzyuba, A.V. Saveliev, V.I. Konov, E. Goovaerts, Nanodiamond photoemitters based on strong narrow-band luminescence from silicon-vacancy defects, Adv. Mater. 21 (2009) 808–812.
[54] A. Sahu, L.J. Qi, M.S. Kang, D.N. Deng, D.J. Norris, Facile synthesis of silver chalcogenide (Ag(2)E; E = Se, S, Te) semiconductor nanocrystals, J. Am. Chem. Soc. 133 (2011) 6509–6512.
[55] M. Yarema, S. Pichler, M. Sytnyk, R. Seyrkammer, R.T. Lechner, G. Fritz-Popovski, D. Jarzab, K. Szendrei, R. Resel, O. Korovyanko, M.A. Loi, O. Paris, G. Hesser, W. Heiss, Infrared emitting and photoconducting colloidal silver chalcogenide nanocrystal quantum dots from a silylamide-promoted synthesis, ACS Nano 5 (2011) 3758–3765.
[56] S.L. Shen, Y.J. Zhang, L. Peng, Y.P. Du, Q.B. Wang, Matchstick-shaped Ag2S–ZnS heteronanostructures preserving both UV/blue and near-infrared photoluminescence, Angew. Chem. Int. Ed. 50 (2011) 7115–7118.
[57] B. Mahler, N. Lequeux, B. Dubertret, Ligand-controlled polytypism of thick-shell CdSe/CdS nanocrystals, J. Am. Chem. Soc. 132 (2010) 953–959.
[58] A.L. Rogach, T. Franzl, T.A. Klar, J. Feldmann, N. Gaponik, V. Lesnyak, A. Shavel, A. Eychmuller, Y.P. Rakovich, J.F. Donegan, Aqueous synthesis of thiol-capped CdTe nanocrystals: state-of-the-art, J. Phys. Chem. C 111 (2007) 14628–14637.
[59] Y.A. Yang, H.M. Wu, K.R. Williams, Y.C. Cao, Synthesis of CdSe and CdTe nanocrystals without precursor injection, Angew. Chem. Int. Ed. 44 (2005) 6712–6715.
[60] S.A. Ivanov, A. Piryatinski, J. Nanda, S. Tretiak, K.R. Zavadil, W.O. Wallace, D. Werder, V.I. Klimov, Type-II core/shell CdS/ZnSe nanocrystals: synthesis, electronic structures, and spectroscopic properties, J. Am. Chem. Soc. 129 (2007) 11708–11719.
[61] A.M. Smith, S.M. Nie, Bright and compact alloyed quantum dots with broadly tunable near-infrared absorption and fluorescence spectra through mercury cation exchange, J. Am. Chem. Soc. 133 (2011) 24–26.
[62] S.D. Miao, S.G. Hickey, B. Rellinghaus, C. Waurisch, A. Eychmuller, Synthesis and characterization of cadmium phosphide quantum dots emitting in the visible red to near-infrared, J. Am. Chem. Soc. 132 (2010) 5613–5615.
[63] R.G. Xie, J.X. Zhang, F. Zhao, W.S. Yang, X.G. Peng, Synthesis of monodisperse, highly emissive, and size-tunable Cd(3)P(2) nanocrystals, Chem. Mater. 22 (2010) 3820–3822.
[64] D.K. Harris, P.M. Allen, H.S. Han, B.J. Walker, J.M. Lee, M.G. Bawendi, Synthesis of cadmium arsenide quantum dots luminescent in the infrared, J. Am. Chem. Soc. 133 (2011) 4676–4679.
[65] I. Kang, F.W. Wise, Electronic structure and optical properties of PbS and PbSe quantum dots, J. Opt. Soc. Am. B: Opt. Phys. 14 (1997) 1632–1646.
[66] F.W. Wise, Lead salt quantum dots: the limit of strong quantum confinement, Acc. Chem. Res. 33 (2000) 773–780.
[67] I. Moreels, Y. Justo, B. De Geyter, K. Haustraete, J.C. Martins, Z. Hens, Size-tunable, bright, and stable PbS quantum dots: a surface chemistry study, ACS Nano 5 (2011) 2004–2012.
[68] B.L. Wehrenberg, C.J. Wang, P. Guyot-Sionnest, Interband and intraband optical studies of PbSe colloidal quantum dots, J. Phys. Chem. B 106 (2002) 10634–10640.
[69] J.M. Pietryga, D.J. Werder, D.J. Williams, J.L. Casson, R.D. Schaller, V.I. Klimov, J.A. Hollingsworth, Utilizing the lability of lead selenide to produce heterostructured nanocrystals with bright, stable infrared emission, J. Am. Chem. Soc. 130 (2008) 4879–4885.
[70] A.A. Guzelian, J.E.B. Katari, A.V. Kadavanich, U. Banin, K. Hamad, E. Juban, A.P. Alivisatos, R.H. Wolters, C.C. Arnold, J.R. Heath, Synthesis of size-selected, surface-passivated InP nanocrystals, J. Phys. Chem. 100 (1996) 7212–7219.
[71] O.I. Micic, A.J. Nozik, Synthesis and characterization of binary and ternary III–V quantum dots, J. Lumin. 70 (1996) 95–107.
[72] A.A. Guzelian, U. Banin, A.V. Kadavanich, X. Peng, A.P. Alivisatos, Colloidal chemical synthesis and characterization of InAs nanocrystal quantum dots, Appl. Phys. Lett. 69 (1996) 1432–1434.
[73] R. Xie, D. Battaglia, X. Peng, Colloidal InP nanocrystals as efficient emitters covering blue to near-infrared, J. Am. Chem. Soc. 129 (2007) 15432–15433.
[74] A. Aharoni, T. Mokari, I. Popov, U. Banin, Synthesis of InAs/CdSe/ZnSe core/shell1/shell2 structures with bright and stable near-infrared fluorescence, J. Am. Chem. Soc. 128 (2006) 257–264.
[75] R.G. Xie, X.G. Peng, Synthetic scheme for high-quality InAs nanocrystals based on self-focusing and one-pot synthesis of InAs-based core–shell nanocrystals, Angew. Chem. Int. Ed. 47 (2008) 7677–7680.
[76] J.P. Zimmer, S.W. Kim, S. Ohnishi, E. Tanaka, J.V. Frangioni, M.G. Bawendi, Size series of small indium arsenide-zinc selenide core–shell nanocrystals and their application to in vivo imaging, J. Am. Chem. Soc. 128 (2006) 2526–2527.
[77] Y.W. Cao, U. Banin, Growth and properties of semiconductor core/shell nanocrystals with InAs cores, J. Am. Chem. Soc. 122 (2000) 9692–9702.
[78] P.M. Allen, M.G. Bawendi, Ternary I–III–VI quantum dots luminescent in the red to near-infrared, J. Am. Chem. Soc. 130 (2008) 9240–9421.
[79] K. Nose, T. Omata, S. Otsuka-Yao-Matsuo, Colloidal synthesis of ternary copper indium diselenide quantum dots and their optical properties, J. Phys. Chem. C 113 (2009) 3455–3460.
[80] R.G. Xie, M. Rutherford, X.G. Peng, Formation of high-quality I–III–VI semiconductor nanocrystals by tuning relative reactivity of cationic precursors, J. Am. Chem. Soc. 131 (2009) 5691–5697.
[81] H.Z. Zhong, Y. Zhou, M.F. Ye, Y.J. He, J.P. Ye, C. He, C.H. Yang, Y.F. Li, Controlled synthesis and optical properties of colloidal ternary chalcogenide CuInS2 nanocrystals, Chem. Mater. 20 (2008) 6434–6443.
[82] H. Zhong, S.S. Lo, T. Mirkovic, Y. Li, Y. Ding, Y. Li, G.D. Scholes, Noninjection gram-scale synthesis of monodisperse pyramidal CuInS(2) nanocrystals and their size-dependent properties, ACS Nano 4 (2010) 5253–5262.
[83] H. Zhong, Z. Wang, E. Bovero, Z. Lu, F.C.J.M. van Veggel, G.D. Scholes, Colloidal CuInSe(2) nanocrystals in the quantum confinement regime: synthesis, optical properties, and electroluminescence, J. Phys. Chem. C 115 (2011) 12396–12402.
[84] D.E. Nam, W.S. Song, H. Yang, Noninjection, one-pot synthesis of Cu-deficient CuInS(2)/ZnS core/shell quantum dots and their fluorescent properties, J. Colloid Interface Sci. 361 (2011) 491–496.
[85] T. Omata, K. Nose, S. Otsuka-Yao-Matsuo, Size dependent optical band gap of ternary I–III–VI(2) semiconductor nanocrystals, J. Appl. Phys. 105 (2009).
[86] X.S. Tang, W.L. Cheng, E.S.G. Choo, J.M. Xue, Synthesis of CuInS(2)–ZnS alloyed nanocubes with high luminescence, Chem. Commun. 47 (2011) 5217–5219.
[87] K.T. Yong, I. Roy, R. Hu, H. Ding, H.X. Cai, J. Zhu, X.H. Zhang, E.J. Bergey, P.N. Prasad, Synthesis of ternary CuInS(2)/ZnS quantum dot bioconjugates and their applications for targeted cancer bioimaging, Integr. Biol. UK 2 (2010) 121–129.
[88] L.A. Li, A. Pandey, D.J. Werder, B.P. Khanal, J.M. Pietryga, V.I. Klimov, Efficient synthesis of highly luminescent copper indium sulfide-based core/shell nanocrystals with surprisingly long-lived emission, J. Am. Chem. Soc. 133 (2011) 1176–1179.
[89] J. Park, C. Dvoracek, K.H. Lee, J.F. Galloway, H.-E.C. Bhang, M.G. Pomper, P.C. Searson, CuInSe/ZnS core/shell NIR quantum dots for biomedical imaging, Small 7 (2011) 3148–3152.
[90] D.J. Norris, A.L. Efros, S.C. Erwin, Doped nanocrystals, Science 319 (2008) 1776–1779.
[91] R.G. Xie, X.G. Peng, Synthesis of Cu-doped InP nanocrystals (d-dots) with ZnSe diffusion barrier as efficient and color-tunable NIR emitters, J. Am. Chem. Soc. 131 (2009) 10645–10651.
[92] I.L. Medintz, H.T. Uyeda, E.R. Goldman, H. Mattoussi, Quantum dot bioconjugates for imaging, labelling and sensing, Nat. Mater. 4 (2005) 435–446.
[93] F. Zhang, E. Lees, F. Amin, P. Rivera Gil, F. Yang, P. Mulvaney, W.J. Parak, Polymer-coated nanoparticles: a universal tool for biolabelling experiments, Small 7 (2011) 3113–3127.
[94] W.R. Algar, D.E. Prasuhn, M.H. Stewart, T.L. Jennings, J.B. Blanco-Canosa, P.E. Dawson, I.L. Medintz, The controlled display of biomolecules on nanoparticles: a challenge suited to bioorthogonal chemistry, Bioconjug. Chem. 22 (2011) 825–858.
[95] X.Y. Wu, H.J. Liu, J.Q. Liu, K.N. Haley, J.A. Treadway, J.P. Larson, N.F. Ge, F. Peale, M.P. Bruchez, Immunofluorescent labeling of cancer marker Her2 and other cellular targets with semiconductor quantum dots, Nat. Biotechnol. 21 (2003) 41–46.
[96] B. Dubertret, P. Skourides, D.J. Norris, V. Noireaux, A.H. Brivanlou, A. Libchaber, In vivo imaging of quantum dots encapsulated in phospholipid micelles, Science 298 (2002) 1759–1762.
[97] S. Kim, M.G. Bawendi, Oligomeric ligands for luminescent and stable nanocrystal quantum dots, J. Am. Chem. Soc. 125 (2003) 14652–14653.
[98] K. Susumu, H.T. Uyeda, I.L. Medintz, T. Pons, J.B. Delehanty, H. Mattoussi, Enhancing the stability and biological functionalities of quantum dots via compact multifunctional ligands, J. Am. Chem. Soc. 129 (2007) 13987–13996.
[99] W. Liu, M. Howarth, A.B. Greytak, Y. Zheng, D.G. Nocera, A.Y. Ting, M.G. Bawendi, Compact biocompatible quantum dots functionalized for cellular imaging, J. Am. Chem. Soc. 130 (2008) 1274–1284.
[100] E. Muro, T. Pons, N. Lequeux, A. Fragola, N. Sanson, Z. Lenkei, B. Dubertret, Small and stable sulfobetaine zwitterionic quantum dots for functional live-cell imaging, J. Am. Chem. Soc. 132 (2010) 4556–4557.
[101] K. Susumu, E. Oh, J.B. Delehanty, J.B. Blanco-Canosa, B.J. Johnson, V. Jain, W.J. Hervey, W.R. Algar, K. Boeneman, P.E. Dawson, I.L. Medintz, Multifunctional compact zwitterionic ligands for preparing robust biocompatible semiconductor quantum dots and gold nanoparticles, J. Am. Chem. Soc. 133 (2011) 9480–9496.
[102] M. Darbandi, R. Thomann, T. Nann, Single quantum dots in silica spheres by microemulsion synthesis, Chem. Mater. 17 (2005) 5720–5725.
[103] D. Gerion, F. Pinaud, S.C. Williams, W.J. Parak, D. Zanchet, S. Weiss, A.P. Alivisatos, Synthesis and properties of biocompatible water-soluble silica-coated CdSe/ZnS semiconductor quantum dots, J. Phys. Chem. B 105 (2001) 8861–8871.
[104] Y. Chan, J.P. Zimmer, M. Stroh, J.S. Steckel, R.K. Jain, M.G. Bawendi, Incorporation of luminescent nanocrystals into monodisperse core–shell silica microspheres, Adv. Mater. 16 (2004) 2092–2097.
[105] W.T. Al-Jamal, K.T. Al-Jamal, P.H. Bomans, P.M. Frederik, K. Kostarelos, Functionalized-quantum-dot-liposome hybrids as multimodal nanoparticles for cancer, Small 4 (2008) 1406–1415.
[106] X. Michalet, F.F. Pinaud, L.A. Bentolila, J.M. Tsay, S. Doose, J.J. Li, G. Sundaresan, A.M. Wu, S.S. Gambhir, S. Weiss, Quantum dots for live cells, in vivo imaging, and diagnostics, Science 307 (2005) 538–544.
[107] S. Zurrida, A. Morabito, V. Galimberti, A. Luini, M. Greco, C. Bartoli, R. Raselli, N. Rossi, G. Vessecchia, N. Cascinelli, U. Veronesi, Importance of the level of axillary involvement in relation to traditional variables in the prognosis of breast cancer, Int. J. Oncol. 15 (1999) 475–480.

[108] S. Ohnishi, S.J. Lomnes, R.G. Laurence, A. Gogbashian, G. Mariani, J.V. Frangioni, Organic alternatives to quantum dots for intraoperative near-infrared fluorescent sentinel lymph node mapping, Mol. Imaging 4 (2005) 172–181.
[109] S. Kim, Y.T. Lim, E.G. Soltesz, A.M. De Grand, J. Lee, A. Nakayama, J.A. Parker, T. Mihaljevic, R.G. Laurence, D.M. Dor, L.H. Cohn, M.G. Bawendi, J.V. Frangioni, Near-infrared fluorescent type II quantum dots for sentinel lymph node mapping, Nat. Biotechnol. 22 (2004) 93–97.
[110] E. Tanaka, H.S. Choi, H. Fujii, M.G. Bawendi, J.V. Frangioni, Image-guided oncologic surgery using invisible light: completed pre-clinical development for sentinel lymph node mapping, Ann. Surg. Oncol. 13 (2006) 1671–1681.
[111] C.P. Parungo, Y.L. Colson, S.W. Kim, S. Kim, L.H. Cohn, M.G. Bawendi, J.V. Frangioni, Sentinel lymph node mapping of the pleural space, Chest 127 (2005) 1799–1804.
[112] C.P. Parungo, S. Ohnishi, S.W. Kim, S. Kim, R.G. Laurence, E.G. Soltesz, F.Y. Chen, Y.L. Colson, L.H. Cohn, M.G. Bawendi, J.V. Frangioni, Intraoperative identification of esophageal sentinel lymph nodes with near-infrared fluorescence imaging, J. Thorac. Cardiovasc. Surg. 129 (2005) 844–850.
[113] E.G. Soltesz, S. Kim, S.W. Kim, R.G. Laurence, A.M. De Grand, C.P. Parungo, L.H. Cohn, M.G. Bawendi, J.V. Frangioni, Sentinel lymph node mapping of the gastrointestinal tract by using invisible light, Ann. Surg. Oncol. 13 (2006) 386–396.
[114] S.W. Kim, J.P. Zimmer, S. Ohnishi, J.B. Tracy, J.V. Frangioni, M.G. Bawendi, Engineering InAs(x)P(1 − x)/InP/ZnSe III–V alloyed core/shell quantum dots for the near-infrared, J. Am. Chem. Soc. 127 (2005) 10526–10532.
[115] R.F. Uren, R. Howman-Giles, J.F. Thompson, Patterns of lymphatic drainage from the skin in patients with melanoma, J. Nucl. Med. 44 (2003) 570–582.
[116] B. Ballou, Quantum dot surfaces for use in vivo and in vitro, Curr. Top. Dev. Biol. 70 (2005) 103–120.
[117] B. Ballou, L.A. Ernst, S. Andreko, T. Harper, J.A. Fitzpatrick, A.S. Waggoner, M.P. Bruchez, Sentinel lymph node imaging using quantum dots in mouse tumor models, Bioconjug. Chem. 18 (2007) 389–396.
[118] E. Pic, T. Pons, L. Bezdetnaya, A. Leroux, F. Guillemin, B. Dubertret, F. Marchal, Fluorescence imaging and whole-body biodistribution of near-infrared-emitting quantum dots after subcutaneous injection for regional lymph node mapping in mice, Mol. Imaging Biol. 12 (2009) 394–405.
[119] J.D. Smith, G.W. Fisher, A.S. Waggoner, P.G. Campbell, The use of quantum dots for analysis of chick CAM vasculature, Microvasc. Res. 73 (2007) 75–83.
[120] B. Ballou, B.C. Lagerholm, L.A. Ernst, M.P. Bruchez, A.S. Waggoner, Noninvasive imaging of quantum dots in mice, Bioconjug. Chem. 15 (2004) 79–86.
[121] F. Duconge, T. Pons, C. Pestourie, L. Herin, B. Theze, K. Gombert, B. Mahler, F. Hinnen, B. Kuhnast, F. Dolle, B. Dubertret, B. Tavitian, Fluorine-18-labeled phospholipid quantum dot micelles for in vivo multimodal imaging from whole body to cellular scales, Bioconjug. Chem. 19 (2008) 1921–1926.
[122] M.L. Schipper, Z. Cheng, S.W. Lee, L.A. Bentolila, G. Iyer, J. Rao, X. Chen, A.M. Wu, S. Weiss, S.S. Gambhir, microPET-based biodistribution of quantum dots in living mice, J. Nucl. Med. 48 (2007) 1511–1518.
[123] D.E. Owens 3rd, N.A. Peppas, Opsonization, biodistribution, and pharmacokinetics of polymeric nanoparticles, Int. J. Pharm. 307 (2006) 93–102.
[124] T.J. Daou, L. Li, P. Reiss, V. Josserand, I. Texier, Effect of poly(ethylene glycol) length on the in vivo behavior of coated quantum dots, Langmuir 25 (2009) 3040–3044.
[125] J.A.J. Fitzpatrick, S.K. Andreko, L.A. Ernst, A.S. Waggoner, B. Ballou, M.P. Bruchez, Long-term persistence and spectral blue shifting of quantum dots in vivo, Nano Lett. 9 (2009) 2736–2741.
[126] M. Vibin, R. Vinayakan, A. John, V. Raji, C.S. Rejiya, A. Abraham, Biokinetics and in vivo distribution behaviours of silica-coated cadmium selenide quantum dots, Biol. Trace Elem. Res. 142 (2011) 213–222.
[127] S. Bonvalot, R. Miceli, M. Berselli, S. Causeret, C. Colombo, L. Mariani, H. Bouzaiene, C. Le Pechoux, P.G. Casali, A. Le Cesne, M. Fiore, A. Gronchi, Aggressive surgery in retroperitoneal soft tissue sarcoma carried out at high-volume centers is safe and is associated with improved local control, Ann. Surg. Oncol. 17 (2010) 1507–1514.
[128] W. Stummer, U. Pichlmeier, T. Meinel, O.D. Wiestler, F. Zanella, R. Hans-Jurgen, A.-G.S. Grp, Fluorescence-guided surgery with 5-aminolevulinic acid for resection of malignant glioma: a randomised controlled multicentre phase III trial, Lancet Oncol. 7 (2006) 392–401.
[129] Y. Matsumura, H. Maeda, A New concept for macromolecular therapeutics in cancer-chemotherapy — mechanism of tumoritropic accumulation of proteins and the antitumor agent Smancs, Cancer Res. 46 (1986) 6387–6392.
[130] R.K. Jain, Transport of molecules, particles, and cells in solid tumors, Ann. Rev. Biomed. Eng. 1 (1999) 241–263.
[131] X.H. Gao, Y.Y. Cui, R.M. Levenson, L.W.K. Chung, S.M. Nie, In vivo cancer targeting and imaging with semiconductor quantum dots, Nat. Biotechnol. 22 (2004) 969–976.
[132] A. Papagiannaros, T. Levchenko, W. Hartner, D. Mongayt, V. Torchilin, Quantum dots encapsulated in phospholipid micelles for imaging and quantification of tumors in the near-infrared region, Nanomed. Nanotechnol. 5 (2009) 216–224.
[133] Z. Popovic, W.H. Liu, V.P. Chauhan, J. Lee, C. Wong, A.B. Greytak, N. Insin, D.G. Nocera, D. Fukumura, R.K. Jain, M.G. Bawendi, A nanoparticle size series for in vivo fluorescence imaging, Angew. Chem. Int. Ed. 49 (2010) 8649–8652.
[134] V.P. Chauhan, Z. Popović, O. Chen, J. Cui, D. Fukumura, M.G. Bawendi, R.K. Jain, Fluorescent nanorods and nanospheres for real-time in vivo probing of nanoparticle shape-dependent tumor penetration, Angew. Chem. Int. Ed. 50 (2011) 11417–11420.
[135] S.D. Perrault, C. Walkey, T. Jennings, H.C. Fischer, W.C.W. Chan, Mediating tumor targeting efficiency of nanoparticles through design, Nano Lett. 9 (2009) 1909–1915.
[136] M.E. Akerman, W.C.W. Chan, P. Laakkonen, S.N. Bhatia, E. Ruoslahti, Nanocrystal targeting in vivo, Proc. Natl. Acad. Sci. U. S. A. 99 (2002) 12617–12621.
[137] S.H. Bhang, N. Won, T.J. Lee, H. Jin, J. Nam, J. Park, H. Chung, H.S. Park, Y.E. Sung, S.K. Hahn, B.S. Kim, S. Kim, Hyaluronic acid-quantum dot conjugates for in vivo lymphatic vessel imaging, ACS Nano 3 (2009) 1389–1398.
[138] A. Jayagopal, P.K. Russ, F.R. Haselton, Surface engineering of quantum dots for in vivo vascular Imaging, Bioconjug. Chem. 18 (2007) 1424–1433.
[139] R. Kikkeri, B. Lepenies, A. Adibekian, P. Laurino, P.H. Seeberger, In vitro imaging and in vivo liver targeting with carbohydrate capped quantum dots, J. Am. Chem. Soc. 131 (2009) 2110–2112.
[140] X.F. Yu, L.D. Chen, K.Y. Li, Y. Li, S. Xiao, X. Luo, J. Liu, L. Zhou, Y.L. Deng, D.W. Pang, Q.Q. Wang, Immunofluorescence detection with quantum dot bioconjugates for hepatoma in vivo, J. Biomed. Opt. 12 (2007).
[141] H. Tada, H. Higuchi, T.M. Wanatabe, N. Ohuchi, In vivo real-time tracking of single quantum dots conjugated with monoclonal anti-HER2 antibody in tumors of mice, Cancer Res. 67 (2007) 1138–1144.
[142] L.L. Yang, H. Mao, Y.A. Wang, Z.H. Cao, X.H. Peng, X.X. Wang, H.W. Duan, C.C. Ni, Q.G. Yuan, G. Adams, M.Q. Smith, W.C. Wood, X.H. Gao, S.M. Nie, Single chain epidermal growth factor receptor antibody conjugated nanoparticles for in vivo tumor targeting and imaging, Small 5 (2009) 235–243.
[143] D.S. Lidke, P. Nagy, R. Heintzmann, D.J. Arndt-Jovin, J.N. Post, H.E. Grecco, E.A. Jares-Erijman, T.M. Jovin, Quantum dot ligands provide new insights into erbB/HER receptor-mediated signal transduction, Nat. Biotechnol. 22 (2004) 198–203.
[144] P. Diagaradjane, J.M. Orenstein-Cardona, N.E. Colon-Casasnovas, A. Deorukhkar, S. Shentu, N. Kuno, D.L. Schwartz, J.G. Gelovani, S. Krishnan, Imaging epidermal growth factor receptor expression in vivo: Pharmacokinetic and biodistribution characterization of a bioconjugated quantum dot nanoprobe, Clin. Cancer Res. 14 (2008) 731–741.
[145] W.B. Cai, D.W. Shin, K. Chen, O. Gheysens, Q.Z. Cao, S.X. Wang, S.S. Gambhir, X.Y. Chen, Peptide-labeled near-infrared quantum dots for imaging tumor vasculature in living subjects, Nano Lett. 6 (2006) 669–676.
[146] B.R. Smith, Z. Cheng, A. De, A.L. Koh, R. Sinclair, S.S. Gambhir, Real-time intravital imaging of RGD-quantum dot binding to luminal endothelium in mouse tumor neovasculature, Nano Lett. 8 (2008) 2599–2606.
[147] H.S. Choi, W.H. Liu, F.B. Liu, K. Nasr, P. Misra, M.G. Bawendi, J.V. Frangioni, Design considerations for tumour-targeted nanoparticles, Nat. Nanotechnol. 5 (2010) 42–47.
[148] X.L. Gao, J. Chen, J.Y. Chen, B.X. Wu, H.Z. Chen, X.G. Jiang, Quantum dots bearing lectin-functionalized nanoparticles as a platform for in vivo brain imaging, Bioconjug. Chem. 19 (2008) 2189–2195.
[149] K.C. Weng, C.O. Noble, B. Papahadjopoulos-Sternberg, F.F. Chen, D.C. Drummond, D.B. Kirpotin, D.H. Wang, Y.K. Hom, B. Hann, J.W. Park, Targeted tumor cell internalization and imaging of multifunctional quantum dot-conjugated immunoliposomes in vitro and in vivo, Nano Lett. 8 (2008) 2851–2857.
[150] J. Nicolas, D. Brambilla, O. Carion, T. Pons, I. Maksimovic, E. Larquet, B. Le Droumaguet, K. Andrieux, B. Dubertret, P. Couvreur, Quantum dot-loaded PEGylated poly(alkyl cyanoacrylate) nanoparticles for in vitro and in vivo imaging, Soft Matter 7 (2011) 6187–6193.
[151] Y. Lei, H. Tang, L. Yao, R. Yu, M. Feng, B. Zou, Applications of mesenchymal stem cells labeled with Tat peptide conjugated quantum dots to cell tracking in mouse body, Bioconjug. Chem. 19 (2008) 421–427.
[152] E.B. Voura, J.K. Jaiswal, H. Mattoussi, S.M. Simon, Tracking metastatic tumor cell extravasation with quantum dot nanocrystals and fluorescence emission-scanning microscopy, Nat. Med. 10 (2004) 993–998.
[153] A. Jayagopal, Y.R. Su, J.L. Blakemore, M.F. Linton, S. Fazio, F.R. Haselton, Quantum dot mediated imaging of atherosclerosis, Nanotechnology 20 (2009).
[154] A. Hoshino, K. Hanaki, K. Suzuki, K. Yamamoto, Applications of T-lymphoma labeled with fluorescent quantum dots to cell tracing markers in mouse body, Biochem. Biophys. Res. Commun. 314 (2004) 46–53.
[155] C.M. Shi, Y. Zhu, Z.H. Xie, W.P. Qian, C.L. Hsieh, S.M. Nie, Y.P. Su, H.E. Zhau, L.W.K. Chung, Visualizing human prostate cancer cells in mouse skeleton using bioconjugated near-infrared fluorescent quantum dots, Urology 74 (2009) 446–451.
[156] M. Stroh, J.P. Zimmer, D.G. Duda, T.S. Levchenko, K.S. Cohen, E.B. Brown, D.T. Scadden, V.P. Torchilin, M.G. Bawendi, D. Fukumura, R.K. Jain, Quantum dots spectrally distinguish multiple species within the tumor milieu in vivo, Nat. Med. 11 (2005) 678–682.
[157] A.Y. Louie, Multimodality imaging probes: design and challenges, Chem. Rev. 110 (2010) 3146–3195.
[158] W.J.M. Mulder, R. Koole, R.J. Brandwijk, G. Storm, P.T.K. Chin, G.J. Strijkers, C.D. Donega, K. Nicolay, A.W. Griffioen, Quantum dots with a paramagnetic coating as a bimodal molecular imaging probe, Nano Lett. 6 (2006) 1–6.
[159] W.J.M. Mulder, K. Castermans, J.R. van Beijnum, M.G.A.O. Egbrink, P.T.K. Chin, Z.A. Fayad, C.W.G.M. Lowik, E.L. Kaijzel, I. Que, G. Storm, G.J. Strijkers, A.W. Griffioen, K. Nicolay, Molecular imaging of tumor angiogenesis using alpha v beta 3-integrin targeted multimodal quantum dots, Angiogenesis 12 (2009) 17–24.
[160] S. Wang, B.R. Jarrett, S.M. Kauzlarich, A.Y. Louie, Core/shell quantum dots with high relaxivity and photoluminescence for multimodality imaging, J. Am. Chem. Soc. 129 (2007) 3848–3856.
[161] K.T. Yong, Mn-doped near-infrared quantum dots as multimodal targeted probes for pancreatic cancer imaging, Nanotechnology 20 (2009).
[162] L. Li, E.S.G. Choo, Z. Liu, J. Ding, J. Xue, Double-layer silica core–shell nanospheres with superparamagnetic and fluorescent functionalities, Chem. Phys. Lett. 461 (2008) 114–117.

[163] B. Zhang, J. Cheng, X. Gong, X. Dong, X. Liu, G. Ma, J. Chang, Facile fabrication of multi-colors high fluorescent/superparamagnetic nanoparticles, J. Colloid Interface Sci. 322 (2008) 485–490.
[164] R. Wilson, D.G. Spiller, I.A. Prior, R. Bhatt, A. Hutchinson, Magnetic microspheres encoded with photoluminescent quantum dots for multiplexed detection, J. Mater. Chem. 17 (2007) 4400–4406.
[165] J.-S. Choi, Y.-W. Jun, S.-I. Yeon, H.C. Kim, J.-S. Shin, J. Cheon, Biocompatible heterostructured nanoparticles for multimodal biological detection, J. Am. Chem. Soc. 128 (2006) 15982–15983.
[166] G. van Dam, G. Themelis, L. Crane, N. Harlaar, R. Pleijhuis, W. Kelder, A. Sarantopoulos, J. de Jong, H. Arts, A. van der Zee, J. Bart, P. Low, V. Ntziachristos, Intraoperative tumor-specific fluorescence imaging in ovarian cancer by folate receptor-α targeting: first in-human results, Nat. Med. 17 (2011) 1315–1319.
[167] D. Pan, L. An, Z. Sun, W. Hou, Y. Yang, Z. Yang, Y. Lu, Synthesis of Cu–In–S ternary nanocrystals with tunable structure and composition, J. Am. Chem. Soc. 130 (2008) 5620–5621.